UNIVERSIDAD DE CONCEPCIÓN

Centro de Investigación en Ingeniería Matemática (CI²MA)

A stabilized displacement - stress formulation for a linear elasticity problema with mixed boundary conditions

Tomás Barrios, Edwin Behrens,
Rommel Bustinza, Jose M. Cascon

PREPRINT 2026-17

SERIE DE PRE-PUBLICACIONES

A stabilized displacement–stress formulation for a linear elasticity problem with mixed boundary conditions

Tomás P. Barrios[1,3], Edwin Behrens[2,3], Rommel Bustinza[4,5], and J. Manuel Cascón[6,7]

[1]Departamento de Matemática y Física Aplicadas, Facultad de Ingeniería, Universidad Católica de la Santísima Concepción, Concepción, Chile, e-mail: tomas@ucsc.cl
[2]Departamento de Ingeniería Civil, Facultad de Ingeniería, Universidad Católica de la Santísima Concepción, Concepción, Chile , e-mail: ebehrens@ucsc.cl
[3]Grupo de Investigación en Análisis Numérico y Cálculo Científico, GIANuC^2, Concepción, Chile.
[4]Corresponding author. Departamento de Ingeniería Matemática, Universidad de Concepción, Concepción, Chile, e-mail: rbustinza@udec.cl
[5]Centro de Investigación en Ingeniería Matemática, CI^{2}MA, Concepción, Chile.
[6]Departamento de Economía e Historia Económica, Facultad de Economía, Universidad de Salamanca, Salamanca, Spain, e-mail: casbar@usal.es
[7]Instituto Universitario de Física Fundamental y Matemáticas, IUFFM, Salamanca, Spain.

Abstract

We consider the linear elasticity problem with mixed boundary conditions and introduce an stabilized mixed scheme, locking free, circumventing the use of the rotation as an additional unknown. We obtain optimal a priori error estimate and develop the corresponding a posteriori error analysis, endowing the scheme with an estimator that is reliable and locally efficient. We provide numerical experiments that illustrate the performance of the corresponding adaptive algorithm and support its use in practice.

Mathematics Subject Classifications (1991): 65N15, 65N30, 65N50, 74B05, 74S05

Key words: A posteriori error estimates, mixed finite element, augmented formulation, linear elasticity, Ritz projection

1 Introduction

Normally, in order to avoid the effects of locking in linear elasticity, the mixed finite element method is employed. We point out that this approach allows us to approximate additional unknowns of physical interest (such as the stress, the rotation, for e.g.), simultaneously (see [22, 21, 4, 6]). Nevertheless,

it is well known that stabilized mixed finite element method for the linear elasticity problem involves many degrees of freedom (see [4, 5]).

The application of stabilization techniques have the advantage that they allows us to use simpler finite element subspaces, including equal-order interpolations, which are highly desired since they simplify the coding, but they are generally unstable within the mixed approach.

In particular, the popularity of the mixed method based on the Hellinger and Reissner formulation, that is, an scheme approximating simultaneously the displacement and the Cauchy stress tensor, is supported by the fact that being a locking-free scheme, it improves the approximation of the stress (see [3, 33]). Usually, the symmetry of the Cauchy stress tensor is weakly imposed through the introduction of rotation as a new unknown, increasing the number of degrees of freedom (see [6]). Recently, in [2], following the ideas introduced in [23], an alternative procedure is described, which is based on the use of a skew symmetric tensor instead of the symmetric deformation tensor, thus we can circumvent the use of rotation, allowing to reduce the number of unknowns (also see [8, 14]).

From a practical point of view, mixed boundary conditions describe many situations of interest. On the contrary, they have only been treated in the works [28, 1, 31, 8]. In [28], in the case of mixed boundary conditions, the Neumann boundary condition is imposed weakly, through the use of a new unknown that can be interpreted as the trace of the displacement on the Neumann boundary. This technique entails some difficulties since the resulting variational formulation has a saddle-point structure. More specifically, the scheme is augmented by adding least squares terms multiplied by some positive parameters, looking for its admisible values, in order to ensure strong coercivity of the resulting bilinear form to fullfill the hypotheses of the Babuška–Brezzi theory. One difficulty here is that one parameter depends on Korn's constant, which generally only its existence is known, but not its exact value. In addition the discrete scheme requires the use of an independent mesh of the Neumann boundary that has to satisfy a compatibility condition with the mesh induced by the triangulation of the domain (see [29]). However, to the best of our knowledge, these criteria are only established for 2D, i.e. for 3D there are no criteria available to build the aforementioned independent mesh of the Neumann boundary. This was fixed in [31] imposing the Neumann boundary condition in a strong sense, where the resulting scheme is well-posed and free of locking, allowing to approximate the stress, the displacement and the rotation, for both 2D and 3D, but the problem of the dependence of a parameter on the Korn-type constant, persists. In addition, the primal formulation with mixed boundary conditions is studied in [1]. Alternatively, for the equations describing the incompressible elasticity model formulated using a mixed approach, in [8] the treatment of the Neumann's condition is done through the use of a homogenization technique, which is valid for 2D and 3D, and its stabilization parameters do not depend on unknown constants.

Concerning the a posteriori error analysis in elasticity, we can mention the classical works [24, 35]. In regards to a stabilized scheme, an a posteriori error estimator of residual type has been derived in [19] in the case of pure homogeneous Dirichlet boundary conditions, whose analysis has been extended to the case of non-homogeneous Dirichlet and mixed boundary conditions in [11]. Although this a posteriori error estimator is reliable and efficient, its computation could be expensive, specially if one thinks in its extension to the three-dimensional case. This motivated the development of subsequent works [12, 13], which are based on the boundedness of the solution of the Ritz projection of the error. The estimators presented there do not involve either tangential or normal jumps, so, from a practical

point of view, they are cheaper and easier to implement, compared to those previously developed in [19, 11]. A posteriori error analysis based on the Ritz projection of the error has been extended in other directions. For example, an a posteriori error estimator for Darcy flow has been developed in [15, 16], while another one for the Stokes system can be found in [7] as well as for Oseen equations in [17, 18].

The aim of this paper is to extend the applicability of [2] to the case of mixed boundary conditions, that works for both two and three-dimensional cases. More specifically, our interest in this article is focus in both error analysis, i.e., a priori and a posteriori. As usual, the a priori error analysis is based on additional regularity and the corresponding approximations properties of the finite element spaces, whereas for the a posteriori error analysis, our analysis is based on the Ritz projection of the error. We obtain an a posteriori error estimator that is reliable and locally efficient. Moreover, numerical experiments support the use of the new a posteriori error estimates in practice.

The rest of the paper is organized as follows. In Section 2, we introduce the augmented variational formulation for the linear elasticity problem with mixed boundary conditions, the corresponding Galerkin scheme and the simplest finite element subspaces that can be used. In Section 3, we develop the a posteriori error analysis and propose the new a posteriori error estimator. Finally, in Section 4 we provide several numerical experiments that support the use of the new a posteriori error estimates in practice.

We end this section with some notations to be used throughout the paper. Given $d \in \{2,3\}$ and a Hilbert space H, we denote by H^d (resp. $H^{d\times d}$) the space of vectors (resp. square tensors of order d) with entries in H. Given $\boldsymbol{\tau} := (\tau_{ij})$ and $\boldsymbol{\zeta} := (\zeta_{ij}) \in \mathbb{R}^{d\times d}$, we denote $\boldsymbol{\tau}^t := (\tau_{ji})$, $\mathrm{tr}(\boldsymbol{\tau}) := \tau_{11} + \cdots + \tau_{dd}$ and $\boldsymbol{\tau} : \boldsymbol{\zeta} := \sum_{i,j=1}^{d} \tau_{ij}\zeta_{ij}$. We also use the standard notations for Sobolev spaces and norms. Additionally, we denote by $\boldsymbol{I}$ the identity matrix in $\mathbb{R}^{d\times d}$ and

$$H(\mathbf{div};\Omega) := \{\boldsymbol{\tau} \in [L^2(\Omega)]^{d\times d} : \ \mathbf{div}(\boldsymbol{\tau}) \in [L^2(\Omega)]^d\},$$

$$H_0(\mathbf{div};\Omega) := \left\{\boldsymbol{\tau} \in H(\mathbf{div};\Omega) : \ \int_\Omega \mathrm{tr}(\boldsymbol{\tau}) = 0\right\}.$$

We notice that for any $\boldsymbol{\tau} \in H(\mathbf{div};\Omega)$ there exist a unique $\boldsymbol{\tau}_0 \in H_0(\mathbf{div};\Omega)$ and $\delta := \frac{1}{d|\Omega|}\int_\Omega \mathrm{tr}(\boldsymbol{\tau}) \in \mathbb{R}$ such that $\boldsymbol{\tau} = \boldsymbol{\tau}_0 + \delta \boldsymbol{I}$. Moreover, we introduce the deviator of tensor $\boldsymbol{\tau}$, as $\boldsymbol{\tau}^d := \boldsymbol{\tau} - \frac{1}{d}\mathrm{tr}(\boldsymbol{\tau})I$. Finally, C (with or without subscripts) denote generic constants, independent of the discretization parameters and Lamé constants, that may take different values at different occurrences.

2 Homogeneous mixed boundary condition: A priori and a posteriori error analysis

Let $\Omega \subset \mathbb{R}^d$ be a bounded and simply connected domain with a Lipschitz-continuous boundary Γ, and let Γ_D and Γ_N be two disjoint open subsets of Γ such that $\Gamma = \overline{\Gamma}_D \cup \overline{\Gamma}_N$ and Γ_D has positive measure. We denote by $\mathbb{C}$ the elasticity operator determined by Hooke's law, that is,

$$\mathbb{C}\,\boldsymbol{\zeta} := \lambda\,\mathrm{tr}(\boldsymbol{\zeta})\,\boldsymbol{I} + 2\mu\,\boldsymbol{\zeta}, \qquad \forall\,\boldsymbol{\zeta} \in [L^2(\Omega)]^{d\times d},$$

where $\lambda, \mu > 0$ are the Lamé parameters. It is easy to see that

$$\mathbb{C}^{-1}\boldsymbol{\zeta} := \frac{1}{2\mu}\,\boldsymbol{\zeta} - \frac{\lambda}{2\mu(d\lambda + 2\mu)}\,\mathrm{tr}(\boldsymbol{\zeta})\,\boldsymbol{I}, \qquad \forall\,\boldsymbol{\zeta} \in [L^2(\Omega)]^{d\times d}.$$

Now, assuming we are given a volume force $\boldsymbol{f} \in [L^2(\Omega)]^d$, we consider the problem: find the displacement $\boldsymbol{u}$ and the stress tensor $\boldsymbol{\sigma}$ such that

$$\begin{cases} -\mathbf{div}(\boldsymbol{\sigma}) = \boldsymbol{f} & \text{in } \Omega, \\ \boldsymbol{\sigma} = \mathbb{C}\,\varepsilon(\boldsymbol{u}) & \text{in } \Omega, \\ \boldsymbol{u} = \boldsymbol{0} & \text{on } \Gamma_D, \\ \boldsymbol{\sigma}\boldsymbol{n} = \boldsymbol{0} & \text{on } \Gamma_N, \end{cases} \tag{1}$$

where $\varepsilon(\boldsymbol{u}) := \frac{1}{2}(\nabla\boldsymbol{u} + (\nabla\boldsymbol{u})^t)$ is the strain tensor of small deformations and $\boldsymbol{n}$ is the unit outward normal to Γ. The second equation of (1) clearly shows that $\boldsymbol{\sigma}$ is symmetric.

Proceeding as in [23], we define the skew symmetric tensor $\gamma(\boldsymbol{v}) := \frac{1}{2}(\nabla\boldsymbol{v} - (\nabla\boldsymbol{v})^t)$, for any $\boldsymbol{v} \in [H^1(\Omega)]^d$. As a result, $\varepsilon(\boldsymbol{u}) = \nabla\boldsymbol{u} - \gamma(\boldsymbol{u})$ in Ω, and we rewrite the constitutive equation as

$$\mathbb{C}^{-1}\boldsymbol{\sigma} = \nabla\boldsymbol{u} - \gamma(\boldsymbol{u}) \qquad \text{in } \Omega. \tag{2}$$

The symmetry of the Cauchy stress tensor implies that

$$\int_\Omega \gamma(\boldsymbol{v}) : \boldsymbol{\sigma} = \boldsymbol{0}, \qquad \forall\,\boldsymbol{v} \in [H^1(\Omega)]^d. \tag{3}$$

Let $H_N(\mathbf{div};\Omega) := \{\boldsymbol{\tau} \in H(\mathbf{div};\Omega) :\ \boldsymbol{\tau}\boldsymbol{n} = \boldsymbol{0} \text{ on } \Gamma_N\}$. These equations allow us to introduce the following mixed variational formulation: Find $(\boldsymbol{\sigma}, \boldsymbol{u}) \in H_N(\mathbf{div};\Omega) \times [H^1(\Omega)]^d$ such that

$$\int_\Omega \mathbb{C}^{-1}\boldsymbol{\sigma} : \boldsymbol{\tau} + \int_\Omega \boldsymbol{u}\cdot\mathbf{div}(\boldsymbol{\tau}) + \int_\Omega \gamma(\boldsymbol{u}) : \boldsymbol{\tau} = \boldsymbol{0} \qquad \forall\,\boldsymbol{\tau} \in H_N(\mathbf{div};\Omega), \tag{4}$$

$$-\int_\Omega \boldsymbol{v}\cdot\mathbf{div}(\boldsymbol{\sigma}) - \int_\Omega \gamma(\boldsymbol{v}) : \boldsymbol{\sigma} = \int_\Omega \boldsymbol{f}\cdot\boldsymbol{v} \qquad \forall\,\boldsymbol{v} \in [H^1(\Omega)]^d. \tag{5}$$

Let κ_1 and κ_2 be positive parameters, independent of λ, we include the least squares terms

$$\kappa_1 \int_\Omega (\varepsilon(\boldsymbol{u}) - \mathbb{C}^{-1}\boldsymbol{\sigma}) : (\varepsilon(\boldsymbol{v}) + \mathbb{C}^{-1}\boldsymbol{\tau}) = 0 \qquad \forall\,(\boldsymbol{\tau}, \boldsymbol{v}) \in H(\mathbf{div};\Omega) \times [H^1(\Omega)]^d, \tag{6}$$

$$\kappa_2 \int_\Omega \mathbf{div}(\boldsymbol{\sigma})\cdot\mathbf{div}(\boldsymbol{\tau}) = -\kappa_2 \int_\Omega \boldsymbol{f}\cdot\mathbf{div}(\boldsymbol{\tau}) \qquad \forall\,\boldsymbol{\tau} \in H(\mathbf{div};\Omega). \tag{7}$$

We introduce the spaces

$$[H^1_{\Gamma_D}(\Omega)]^d := \{\boldsymbol{v} \in [H^1(\Omega)]^d :\ \boldsymbol{v} = \boldsymbol{0} \text{ on } \Gamma_D\},$$

$\boldsymbol{H} := H(\mathbf{div};\Omega)\times[H^1(\Omega)]^d$, $\boldsymbol{H}_{\Gamma_D} := H(\mathbf{div};\Omega)\times[H^1_{\Gamma_D}(\Omega)]^d$, $\boldsymbol{H}_N := H_N(\mathbf{div};\Omega)\times[H^1(\Omega)]^d$. and $\boldsymbol{H}_0 := H_N(\mathbf{div};\Omega)\times[H^1_{\Gamma_D}(\Omega)]^d$. Adding (4), (5), (6) and (7) we induce the bilinear form $A:\boldsymbol{H}\times\boldsymbol{H}\to\mathbb{R}$ defined by

$$\begin{aligned}A((\boldsymbol{\sigma},\boldsymbol{u}),(\boldsymbol{\tau},\boldsymbol{v})) := &\int_\Omega \mathbb{C}^{-1}\boldsymbol{\sigma}:\boldsymbol{\tau}+\int_\Omega \boldsymbol{u}\cdot\mathbf{div}(\boldsymbol{\tau})+\int_\Omega \boldsymbol{\tau}:\gamma(\boldsymbol{u})-\int_\Omega \boldsymbol{v}\cdot\mathbf{div}(\boldsymbol{\sigma})-\int_\Omega \boldsymbol{\sigma}:\gamma(\boldsymbol{v})\\ &+\kappa_1\int_\Omega(\varepsilon(\boldsymbol{u})-\mathbb{C}^{-1}\boldsymbol{\sigma}):(\varepsilon(\boldsymbol{v})+\mathbb{C}^{-1}\boldsymbol{\tau})+\kappa_2\int_\Omega \mathbf{div}(\boldsymbol{\sigma})\cdot\mathbf{div}(\boldsymbol{\tau}),\end{aligned}$$

and the linear functional $F:\boldsymbol{H}\to\mathbb{R}$ defined by

$$F(\boldsymbol{\tau},\boldsymbol{v}) := \int_\Omega \boldsymbol{f}\cdot(\boldsymbol{v}-\kappa_2\,\mathbf{div}(\boldsymbol{\tau})).$$

The augmented variational formulation for problem (1) reads: Find $(\boldsymbol{\sigma},\boldsymbol{u})\in\boldsymbol{H}_0$ such that

$$A((\boldsymbol{\sigma},\boldsymbol{u}),(\boldsymbol{\tau},\boldsymbol{v})) = F(\boldsymbol{\tau},\boldsymbol{v}),\qquad \forall\,(\boldsymbol{\tau},\boldsymbol{v})\in\boldsymbol{H}_0. \tag{8}$$

In order to prove that (8) is well posed, we need the following technical lemma.

Lemma 1 *For any $\boldsymbol{\tau}\in H(\mathbf{div};\Omega)$ there exists a constant $c_1\in(0,1]$, depending only on Ω, such that*

$$c_1\|\boldsymbol{\tau}_0\|^2_{0,\Omega}\le\|\boldsymbol{\tau}^d\|^2_{0,\Omega}+\|\mathbf{div}(\boldsymbol{\tau})\|^2_{0,\Omega},$$

where $\boldsymbol{\tau}=\boldsymbol{\tau}_0+\delta\boldsymbol{I}$, with $\boldsymbol{\tau}_0\in H_0(\mathbf{div};\Omega)$ and $\delta\in\mathbb{R}$. In addition, for any $\boldsymbol{\tau}\in H_N(\mathbf{div};\Omega)$, there exists a constant $c_2\in(0,1]$, depending only on Ω and Γ_N, such that

$$c_2\|\boldsymbol{\tau}\|^2_{H(\mathbf{div};\Omega)}\le\|\boldsymbol{\tau}_0\|^2_{H(\mathbf{div};\Omega)}.$$

Proof. See Lemma 2.1 and Lemma 2.2 in [28]. □

For all $(\boldsymbol{\tau},\boldsymbol{v})\in\boldsymbol{H}$ we introduce the norm

$$\|(\boldsymbol{\tau},\boldsymbol{v})\|_{\boldsymbol{H}} := \left(\|\boldsymbol{\tau}\|^2_{H(\mathbf{div};\Omega)}+\|\boldsymbol{v}\|^2_{[H^1(\Omega)]^d}\right)^{1/2}.$$

Lemma 2 *Assume that $\kappa_1\in(0,2\mu)$ and $\kappa_2>0$, both independent of λ. Then there exists a constant $\alpha>0$, independent of λ, such that*

$$A((\boldsymbol{\tau},\boldsymbol{v}),(\boldsymbol{\tau},\boldsymbol{v}))\ge\alpha\,\|(\boldsymbol{\tau},\boldsymbol{v})\|^2_{\boldsymbol{H}},\qquad\forall\,(\boldsymbol{\tau},\boldsymbol{v})\in\boldsymbol{H}_0.$$

Proof. According to the definition of A, for any pair $(\boldsymbol{\tau},\boldsymbol{v})\in\boldsymbol{H}_0$, we obtain

$$A((\boldsymbol{\tau},\boldsymbol{v}),(\boldsymbol{\tau},\boldsymbol{v}))\ge\int_\Omega\mathbb{C}^{-1}\boldsymbol{\tau}:\boldsymbol{\tau}+\kappa_1\|\varepsilon(\boldsymbol{v})\|^2_{0,\Omega}-\kappa_1\|\mathbb{C}^{-1}\boldsymbol{\tau}\|^2_{0,\Omega}+\kappa_2\|\mathbf{div}(\boldsymbol{\tau})\|^2_{0,\Omega}. \tag{9}$$

Moreover,

$$\int_\Omega\mathbb{C}^{-1}\boldsymbol{\tau}:\boldsymbol{\tau}=\frac{1}{2\mu}\|\boldsymbol{\tau}^d\|^2_{0,\Omega}+\frac{1}{d(d\lambda+2\mu)}\|\mathrm{tr}(\boldsymbol{\tau})\|^2_{0,\Omega}, \tag{10}$$

$$\|\mathbb{C}^{-1}\boldsymbol{\tau}\|^2_{0,\Omega}=\frac{1}{(2\mu)^2}\|\boldsymbol{\tau}^d\|^2_{0,\Omega}+\frac{1}{d(d\lambda+2\mu)^2}\|\mathrm{tr}(\boldsymbol{\tau})\|^2_{0,\Omega}. \tag{11}$$

Combining (9), (10) and (11), we deduce

$$\begin{aligned} A((\boldsymbol{\tau},\boldsymbol{v}),(\boldsymbol{\tau},\boldsymbol{v})) &\geq \frac{1}{2\mu}\left(1-\frac{\kappa_1}{2\mu}\right)\|\boldsymbol{\tau}^d\|^2_{0,\Omega}+\frac{1}{d(d\lambda+2\mu)}\left(1-\frac{\kappa_1}{d\lambda+2\mu}\right)\|\mathrm{tr}(\boldsymbol{\tau})\|^2_{0,\Omega} \\ &\quad+\kappa_1\|\varepsilon(\boldsymbol{v})\|^2_{0,\Omega}+\kappa_2\|\mathbf{div}(\boldsymbol{\tau})\|^2_{0,\Omega} \\ &\geq \min\left\{\frac{1}{2\mu}\left(1-\frac{\kappa_1}{2\mu}\right),\frac{\kappa_2}{2}\right\}(\|\boldsymbol{\tau}^d\|^2_{0,\Omega}+\|\mathbf{div}(\boldsymbol{\tau})\|^2_{0,\Omega})+\frac{\kappa_2}{2}\|\mathbf{div}(\boldsymbol{\tau})\|^2_{0,\Omega}+\kappa_1\|\varepsilon(\boldsymbol{v})\|^2_{0,\Omega}. \end{aligned}$$

Defining $\alpha_1=\min\left\{\frac{1}{2\mu}\left(1-\frac{\kappa_1}{2\mu}\right),\frac{\kappa_2}{2}\right\}$ and $\alpha_2=\min\{c_1\alpha_1,\kappa_2/2\}$, and using Lemma 1, we obtain

$$A((\boldsymbol{\tau},\boldsymbol{v}),(\boldsymbol{\tau},\boldsymbol{v}))\geq c_2\alpha_2\|\boldsymbol{\tau}\|^2_{H(\mathbf{div};\Omega)}+\kappa_1\|\varepsilon(\boldsymbol{v})\|^2_{0,\Omega}.$$

Finally, the proof is completed applying Korn's inequality, with $\alpha=\min\{c_2\alpha_2,\kappa_1\kappa_D\}$, where $\kappa_D>0$ is Korn's constant. □

Hereafter, we assume that the stabilization parameters (κ_1,κ_2) satisfy the assumptions of Lemma 2. It is not difficult to see that there exists $M>0$, independent of λ, such that

$$|A((\boldsymbol{\sigma},\boldsymbol{u}),(\boldsymbol{\tau},\boldsymbol{v}))|\leq M\,\|(\boldsymbol{\sigma},\boldsymbol{u})\|_{\boldsymbol{H}}\,\|(\boldsymbol{\tau},\boldsymbol{v})\|_{\boldsymbol{H}},\qquad\forall\,(\boldsymbol{\sigma},\boldsymbol{u}),(\boldsymbol{\tau},\boldsymbol{v})\in\boldsymbol{H}_0.$$

As a consequence, the augmented variational formulation (8) has a unique solution $(\boldsymbol{\sigma},\boldsymbol{u})\in\boldsymbol{H}_0$ and there exists $C>0$, independent of λ, such that

$$\|(\boldsymbol{\sigma},\boldsymbol{u})\|_{\boldsymbol{H}}\leq C\,\|\boldsymbol{f}\|_{[L^2(\Omega)]^d}.$$

Let h be a positive parameter and we consider a finite dimensional subspace $\boldsymbol{H}_{0,h}\subset\boldsymbol{H}_0$. Then, the Galerkin scheme associated to problem (8) reads: find $(\boldsymbol{\sigma}_h,\boldsymbol{u}_h)\in\boldsymbol{H}_{0,h}$ such that

$$A((\boldsymbol{\sigma}_h,\boldsymbol{u}_h),(\boldsymbol{\tau}_h,\boldsymbol{v}_h))=F(\boldsymbol{\tau}_h,\boldsymbol{v}_h),\qquad\forall\,(\boldsymbol{\tau}_h,\boldsymbol{v}_h)\in\boldsymbol{H}_{0,h}.\tag{12}$$

Next we describe the simplest choice of $\boldsymbol{H}_{0,h}$ that preserves stability. We assume that Ω is a polygonal region and let $\{\mathcal{T}_h\}_{h>0}$ be a regular family of triangulations of Ω. Given $T\in\mathcal{T}_h$, we denote by h_T its diameter and define the mesh size $h:=\max\{h_T:\ T\in\mathcal{T}_h\}$. We also assume that each point on $\overline{\Gamma}_D\cap\overline{\Gamma}_N$ is a vertex of $\mathcal{T}_h$ for all $h>0$. Given an integer $\ell\geq 0$ and a subset $S\subset\mathbb{R}^d$, we denote by $P_\ell(S)$ the space of polynomials in d variables defined in S of total degree at most ℓ, and by $\widetilde{P}_\ell(S)$ the space of homogeneous polynomials in d variables defined in S of degree ℓ. For each $T\in\mathcal{T}_h$, the local Raviart–Thomas space of order ℓ is given by

$$RT_\ell(T):=[P_\ell(T)]^d\oplus\widetilde{P}_\ell(T)\,\boldsymbol{x}\subset[P_{\ell+1}(T)]^d,\qquad\boldsymbol{x}=(x_1,\ldots,x_d)^t.$$

Then define the finite element subspaces

$$\boldsymbol{H}_h^{\boldsymbol{\sigma}}:=\{\boldsymbol{\tau}_h\in H(\mathbf{div};\Omega):\ \boldsymbol{\tau}_h|_T\in[RT_\ell(T)^t]^d,\ \forall\,T\in\mathcal{T}_h\},$$

$$\boldsymbol{H}_{N,h}^{\boldsymbol{\sigma}}:=\{\boldsymbol{\tau}_h\in\boldsymbol{H}_h^{\boldsymbol{\sigma}}:\ \boldsymbol{\tau}_h\boldsymbol{n}=\mathbf{0}\text{ on }\Gamma_N\},$$

$$\boldsymbol{H}_h^{\boldsymbol{u}}:=\{\boldsymbol{v}_h\in[C(\overline{\Omega})]^d:\ \boldsymbol{v}_h|_T\in[P_{\ell+1}(T)]^d,\ \forall\,T\in\mathcal{T}_h\},\qquad\boldsymbol{H}_{0,h}^{\boldsymbol{u}}:=\{\boldsymbol{v}_h\in\boldsymbol{H}_h^{\boldsymbol{u}}:\ \boldsymbol{v}_h=0\text{ on }\Gamma_D\}.$$

The simplest choice of stable finite element subspaces (cf. [28]) is

$$\boldsymbol{H}_{0,h}:=\boldsymbol{H}_{N,h}^{\boldsymbol{\sigma}}\times\boldsymbol{H}_{0,h}^{\boldsymbol{u}}.$$

Theorem 3 *Let* $(\boldsymbol{\sigma},\boldsymbol{u}) \in \boldsymbol{H}_0$ *and* $(\boldsymbol{\sigma}_h,\boldsymbol{u}_h) \in \boldsymbol{H}_{0,h}$ *be the unique solutions to problems* (8) *and* (12)*, respectively. Assume that* $\boldsymbol{\sigma} \in [H^r(\Omega)]^{d\times d}$, $\mathbf{div}(\boldsymbol{\sigma}) \in [H^r(\Omega)]^d$ *and* $\boldsymbol{u} \in [H^{r+1}(\Omega)]^d$*, for some* $r \in (0, \ell+1]$*. Then there exists* $C>0$*, independent of* λ *and* h*, such that*

$$\|(\boldsymbol{\sigma},\boldsymbol{u})-(\boldsymbol{\sigma}_h,\boldsymbol{u}_h)\|_{\boldsymbol{H}} \leq C\, h^r \Big(\|\boldsymbol{\sigma}\|_{[H^r(\Omega)]^{d\times d}} + \|\mathbf{div}(\boldsymbol{\sigma})\|_{[H^r(\Omega)]^d} + \|\boldsymbol{u}\|_{[H^{r+1}(\Omega)]^d}\Big).$$

Proof. It relies on Céa's estimate, which is established thanks to the coerciveness of A, and the approximation properties of the finite element subspaces. We omit further details. □

Since the bilinear form associated to (8) has the same definition of the one introduced in Section 2 in [9], straightforward modifications of the a posteriori error analysis developed there, which are related to the considered spaces, allow us to establish that the a posteriori error estimator based on the Ritz projection of the error produces a reliable and locally efficient estimator.

We define the Ritz projection of the error as the unique element $(\bar{\boldsymbol{\sigma}},\bar{\boldsymbol{u}}) \in \boldsymbol{H}_0$ such that for all $(\boldsymbol{\tau},\boldsymbol{v}) \in \boldsymbol{H}_0$,

$$\langle (\bar{\boldsymbol{\sigma}},\bar{\boldsymbol{u}}),(\boldsymbol{\tau},\boldsymbol{v})\rangle_{\boldsymbol{H}} = A((\boldsymbol{\sigma}-\boldsymbol{\sigma}_h,\boldsymbol{u}-\boldsymbol{u}_h),(\boldsymbol{\tau},\boldsymbol{v})), \tag{13}$$

where $\langle\cdot,\cdot\rangle_{\boldsymbol{H}}$ denotes the inner product of $\boldsymbol{H}$, that is,

$$\langle (\boldsymbol{\sigma},\boldsymbol{u}),(\boldsymbol{\tau},\boldsymbol{v})\rangle_{\boldsymbol{H}} := (\boldsymbol{\sigma},\boldsymbol{\tau})_{H(\mathbf{div};\Omega)} + (\boldsymbol{u},\boldsymbol{v})_{[H^1(\Omega)]^d}.$$

Proceeding as in [9], we obtain the a posteriori error indicator

$$\hat{\eta} := \Big(\sum_{T\in\mathcal{T}_h} \hat{\eta}_T^2\Big)^{1/2}, \qquad \hat{\eta}_T^2 := \|\boldsymbol{f}+\mathbf{div}(\boldsymbol{\sigma}_h)\|^2_{[L^2(T)]^d} + \|\varepsilon(\boldsymbol{u}_h)-\mathbb{C}^{-1}\boldsymbol{\sigma}_h\|^2_{[L^2(T)]^{d\times d}}.$$

Theorem 4 *There exist positive constants* $C_{\rm eff}$ *and* $C_{\rm rel}$*, independent of* h *and* λ*, such that*

$$\|(\boldsymbol{\sigma}-\boldsymbol{\sigma}_h,\boldsymbol{u}-\boldsymbol{u}_h)\|_{\boldsymbol{H}} \leq C_{\rm rel}\,\hat{\eta},$$

and for all $T \in \mathcal{T}_h$*,*

$$C_{\rm eff}\hat{\eta}_T \leq \Big(\|\boldsymbol{u}-\boldsymbol{u}_h\|^2_{[H^1(T)]^d} + \|\boldsymbol{\sigma}-\boldsymbol{\sigma}_h\|^2_{H(\mathbf{div};T)}\Big)^{1/2}, \qquad C_{\rm eff} := 2^{-1/2}\min\{1,\mu\}.$$

Proof. The proof follows similar ideas to the given in Section 3 in [9]. □

3 Inhomogeneous mixed boundary condition

In this section, we extend the analysis described in Section 2 to a more general model problem with non homogeneous mixed boundary data. For this purpose, we keep the same geometry and notations introduced before. Next, we introduce the spaces

$$[H^{1/2}_{00}(\Gamma_D)]^d := \{\boldsymbol{v}|_{\Gamma_D} :\ \boldsymbol{v}\in[H^1_{\Gamma_N}(\Omega)]^d\}, \qquad [H^{1/2}_{00}(\Gamma_N)]^d := \{\boldsymbol{v}|_{\Gamma_N} :\ \boldsymbol{v}\in[H^1_{\Gamma_D}(\Omega)]^d\},$$

and denote by $[H^{-1/2}_{00}(\Gamma_N)]^d$ the dual space of $[H^{1/2}_{00}(\Gamma_N)]^d$, with norm $\|\cdot\|_{-1/2,00,\Gamma_N}$.

Given $\boldsymbol{u}_D \in [H^{1/2}_{00}(\Gamma_D)]^d$, $\boldsymbol{g} \in [H^{-1/2}_{00}(\Gamma_N)]^d$ and $\boldsymbol{f} \in [L^2(\Omega)]^d$, we look for the displacement $\tilde{\boldsymbol{u}}$ and the stress $\tilde{\boldsymbol{\sigma}}$ satisfying

$$\begin{cases} -\mathbf{div}(\tilde{\boldsymbol{\sigma}}) = \boldsymbol{f} & \text{in } \Omega, \\ \tilde{\boldsymbol{\sigma}} = \mathbb{C}\,\varepsilon(\tilde{\boldsymbol{u}}) & \text{in } \Omega, \\ \tilde{\boldsymbol{u}} = \boldsymbol{u}_D & \text{on } \Gamma_D, \\ \tilde{\boldsymbol{\sigma}}\boldsymbol{n} = \boldsymbol{g} & \text{on } \Gamma_N. \end{cases} \tag{14}$$

It is not difficult to check that this problem is well-posed. Indeed, since $\boldsymbol{g} \in [H^{-1/2}_{00}(\Gamma_N)]^d$, we set $\tilde{\boldsymbol{\sigma}}_{\boldsymbol{g}} := -\varepsilon(\boldsymbol{z})$, with $\boldsymbol{z} \in [H^1_{\Gamma_D}(\Omega)]^d$ being the unique weak solution of the auxiliary problem

$$-\mathbf{div}(\varepsilon(\boldsymbol{z})) = \mathbf{0} \text{ in } \Omega, \qquad \boldsymbol{z} = \mathbf{0} \text{ on } \Gamma_D, \qquad \varepsilon(\boldsymbol{z})\boldsymbol{n} = \boldsymbol{g} \text{ on } \Gamma_N. \tag{15}$$

Clearly $\tilde{\boldsymbol{\sigma}}_{\boldsymbol{g}} \in H(\mathbf{div};\Omega)$, is divergence-free and satisfies $\tilde{\boldsymbol{\sigma}}_{\boldsymbol{g}}\boldsymbol{n} = -\boldsymbol{g}$ on Γ_N. Moreover, there exists $C_1 > 0$ such that $\|\tilde{\boldsymbol{\sigma}}_{\boldsymbol{g}}\|_{H(\mathbf{div};\Omega)} \leq C_1\|\boldsymbol{g}\|_{-1/2,00,\Gamma_N}$. Now, introducing $\boldsymbol{\sigma} := \tilde{\boldsymbol{\sigma}} + \tilde{\boldsymbol{\sigma}}_{\boldsymbol{g}}$, (14) can be rewritten as

$$\begin{cases} -\mathbf{div}(\boldsymbol{\sigma}) = \boldsymbol{f} & \text{in } \Omega, \\ \boldsymbol{\sigma} - \tilde{\boldsymbol{\sigma}}_{\boldsymbol{g}} = \mathbb{C}\,\varepsilon(\tilde{\boldsymbol{u}}) & \text{in } \Omega, \\ \tilde{\boldsymbol{u}} = \boldsymbol{u}_D & \text{on } \Gamma_D, \\ \boldsymbol{\sigma}\boldsymbol{n} = \mathbf{0} & \text{on } \Gamma_N. \end{cases} \tag{16}$$

Following the procedure described in Section 2 and penalizing the Dirichlet boundary condition, we establish the augmented variational formulation: find $(\boldsymbol{\sigma}, \tilde{\boldsymbol{u}}) \in \boldsymbol{H}_N := H_N(\mathbf{div};\Omega) \times [H^1(\Omega)]^d$ such that

$$\tilde{A}((\boldsymbol{\sigma}, \tilde{\boldsymbol{u}}), (\boldsymbol{\tau}, \boldsymbol{v})) = \tilde{F}(\boldsymbol{\tau}, \boldsymbol{v}), \qquad \forall\, (\boldsymbol{\tau}, \boldsymbol{v}) \in \boldsymbol{H}_N \tag{17}$$

where $\tilde{A} : \boldsymbol{H} \times \boldsymbol{H} :\to \mathbb{R}$ and $\tilde{F} : \boldsymbol{H} :\to \mathbb{R}$ are given by

$$\tilde{A}((\boldsymbol{\zeta}, \boldsymbol{w}), (\boldsymbol{\tau}, \boldsymbol{v})) := A((\boldsymbol{\zeta}, \boldsymbol{w}), (\boldsymbol{\tau}, \boldsymbol{v})) + \int_{\Gamma_D} \boldsymbol{w} \cdot \boldsymbol{v},$$

$$\tilde{F}(\boldsymbol{\tau}, \boldsymbol{v}) := F(\boldsymbol{\tau}, \boldsymbol{v}) + \int_\Omega \mathbb{C}^{-1}\tilde{\boldsymbol{\sigma}}_{\boldsymbol{g}} : \boldsymbol{\tau} - \int_\Omega \boldsymbol{\gamma}(\boldsymbol{v}) : \tilde{\boldsymbol{\sigma}}_{\boldsymbol{g}_h} - \kappa_1 \int_\Omega \mathbb{C}^{-1}\tilde{\boldsymbol{\sigma}}_{\boldsymbol{g}} : (\varepsilon(\boldsymbol{v}) + \mathbb{C}^{-1}\boldsymbol{\tau}) + \int_{\Gamma_D} \boldsymbol{u}_D \cdot \boldsymbol{v}.$$

Straightforward adaptations of Lemma 2 ensures that, considering $\kappa_1 \in (0, 2\mu)$ and $\kappa_2 > 0$, problem (17) is well posed. Defining $\tilde{\boldsymbol{\sigma}} := \boldsymbol{\sigma} - \tilde{\boldsymbol{\sigma}}_{\boldsymbol{g}}$ in Ω, the pair $(\tilde{\boldsymbol{\sigma}}, \tilde{\boldsymbol{u}})$ is a weak solution of (14), and there exists $C > 0$, independent of λ, such that

$$\|(\tilde{\boldsymbol{\sigma}}, \tilde{\boldsymbol{u}})\|_{\boldsymbol{H}} \leq C(\|\boldsymbol{f}\|_{0,\Omega} + \|\boldsymbol{u}_D\|_{1/2,00,\Gamma_D} + \|\boldsymbol{g}\|_{-1/2,00,\Gamma_N}).$$

As usual, the discrete problem inherits these properties for any conforming finite dimensional subspace of $\boldsymbol{H}_N$. Thus, the following discrete problem is well posed: find $(\boldsymbol{\sigma}_h, \tilde{\boldsymbol{u}}_h) \in \boldsymbol{H}_{N,h} := \boldsymbol{H}^{\boldsymbol{\sigma}}_{N,h} \times \boldsymbol{H}^{\boldsymbol{u}}_h$ such that

$$\tilde{A}((\boldsymbol{\sigma}_h, \tilde{\boldsymbol{u}}_h), (\boldsymbol{\tau}_h, \boldsymbol{v}_h)) = \tilde{F}(\boldsymbol{\tau}_h, \boldsymbol{v}_h), \qquad \forall\, (\boldsymbol{\tau}_h, \boldsymbol{v}_h) \in \boldsymbol{H}_{N,h}. \tag{18}$$

For the sake of completeness we present the a-priori error estimate.

Theorem 5 *Let $(\boldsymbol{\sigma}, \tilde{\boldsymbol{u}}) \in \boldsymbol{H}_N$ and $(\boldsymbol{\sigma}_h, \tilde{\boldsymbol{u}}_h) \in \boldsymbol{H}_{N,h}$ be the unique solutions to problems* (17) *and* (18)*, respectively. Assume that $\boldsymbol{\sigma} \in [H^r(\Omega)]^{d\times d}$, $\mathbf{div}(\boldsymbol{\sigma}) \in [H^r(\Omega)]^d$ and $\tilde{\boldsymbol{u}} \in [H^{r+1}(\Omega)]^d$ for some $r \in (0, \ell+1]$. Then there exists $\bar{C}_* > 0$, independent of h, such that*

$$\|(\boldsymbol{\sigma}, \tilde{\boldsymbol{u}}) - (\boldsymbol{\sigma}_h, \tilde{\boldsymbol{u}}_h)\|_{\boldsymbol{H}} \leq \bar{C}_*\, h^r \Big(\|\boldsymbol{\sigma}\|_{r,\Omega} + \|\mathbf{div}(\boldsymbol{\sigma})\|_{r,\Omega} + \|\tilde{\boldsymbol{u}}\|_{r+1,\Omega} \Big).$$

Proof. It is a consequence of Céa's estimate and the corresponding approximation properties. We omit further details. □

Remark 6 *The fact that $\tilde{\boldsymbol{\sigma}}_{\boldsymbol{g}}$ is generally unknown can be remedied by approximating the solution of* (15)*. This allows us to define $\tilde{\boldsymbol{\sigma}}_h := \boldsymbol{\sigma}_h - \varepsilon(\boldsymbol{z}_h)$, with $\boldsymbol{z}_h \in \boldsymbol{H}_h^{\boldsymbol{u}}$ being the solution of the discrete primal formulation associated to* (15)*. Then, assuming that $\boldsymbol{z} \in [H^1_{\Gamma_D}(\Omega) \cap H^{s+1}(\Omega)]^d$ for some $s \in (0, \ell+1]$, and invoking Theorem 5, there exists $C > 0$, independent of h, such that*

$$\|(\tilde{\boldsymbol{\sigma}}, \tilde{\boldsymbol{u}}) - (\tilde{\boldsymbol{\sigma}}_h, \tilde{\boldsymbol{u}}_h)\|_{\boldsymbol{H}} \leq C \Big\{ h^r (\|\boldsymbol{\sigma}\|_{r,\Omega} + \|\mathbf{div}(\boldsymbol{\sigma})\|_{r,\Omega} + \|\tilde{\boldsymbol{u}}\|_{r+1,\Omega}) + h^s \|\boldsymbol{z}\|_{s+1,\Omega} \Big\}.$$

At this point, we remark that in general $\varepsilon(\boldsymbol{z}_h)$ does not belong to $\boldsymbol{H}_{N,h}^{\boldsymbol{\sigma}}$, and requires to compute first $\boldsymbol{z}_h \in \boldsymbol{H}_h^{\boldsymbol{u}}$ in order to calculate it. Clearly, from a computational point of view, this could be expensive. In addition, results to be natural that the way to treat the Dirichlet datum involves the introduction of the nodes lying on Γ_D as unknowns into the system. That is, where the solution is already known, which increases the degrees of freedom of the linear system to be solved. One way to avoid these problems is discussed in the next section.

3.1 An approximation via homogenization of the boundary conditions

To circumvent the difficulties associated with the treatment of non-homogeneous Neumann boundary condition, we follow [16]. First, we let $\mathcal{F}_h$ be the skeleton of $\mathcal{T}_h$, i.e. the list of all the faces (counted once) induced by the triangulation $\mathcal{T}_h$. We decompose $\mathcal{F}_h = \mathcal{F}_h^I \cup \mathcal{F}_h^\partial$ with $\mathcal{F}_h^I := \{F \in \mathcal{F}_h : \ F \subset \Omega\}$ and $\mathcal{F}_h^\partial := \{F \in \mathcal{F}_h : \ F \subset \partial\Omega\}$. We also split $\mathcal{F}_h^\partial = \mathcal{F}_h^D \cup \mathcal{F}_h^N$ where $\mathcal{F}_h^D := \{F \in \mathcal{F}_h^\partial : \ F \subset \Gamma_D\}$ and $\mathcal{F}_h^N := \{F \in \mathcal{F}_h^\partial : \ F \subset \Gamma_N\}$. Hence $\mathcal{F}_h = \mathcal{F}_h^I \cup \mathcal{F}_h^D \cup \mathcal{F}_h^N$.

Now, we approximate the traction datum $\boldsymbol{g}$ by $\boldsymbol{g}_h := \pi_h^\ell(\boldsymbol{g})$ on $\mathcal{F}_h^N$, with $\pi_h^\ell(\boldsymbol{g})$ being the L^2-orthogonal projection of $\boldsymbol{g}$ onto $P_\ell(\mathcal{F}_h^N)$, component-wise. For the Dirichlet datum, we introduce $\boldsymbol{u}_{D,h}$ as a suitable quasi-interpolant of $\boldsymbol{u}_D$ of degree one (obtained first via a Clément type operator and then modified to take into account the boundary condition as in [30, 32]).

Next, in order to approximate the solution of the continuous problem (14), we propose to consider the following problem: find $(\tilde{\boldsymbol{\rho}}, \tilde{\boldsymbol{w}}), \in \boldsymbol{H}$ such that

$$\begin{cases} -\mathbf{div}(\tilde{\boldsymbol{\rho}}) = \boldsymbol{f} & \text{in } \Omega, \\ \tilde{\boldsymbol{\rho}} = \mathbb{C}\,\varepsilon(\tilde{\boldsymbol{w}}) & \text{in } \Omega, \\ \tilde{\boldsymbol{w}} = \boldsymbol{u}_{D,h} & \text{on } \Gamma_D, \\ \tilde{\boldsymbol{\rho}}\boldsymbol{n} = \boldsymbol{g}_h & \text{on } \Gamma_N. \end{cases} \tag{19}$$

In virtue of what has been described at the beginning of the section, it can be established that (19) has a unique solution $(\tilde{\boldsymbol{\rho}}, \tilde{\boldsymbol{w}}) \in \boldsymbol{H}$. In addition, this allows us to establish the existence and uniqueness of $(\boldsymbol{\rho}, \tilde{\boldsymbol{w}}) \in \boldsymbol{H}_N$ and $(\boldsymbol{\rho}_h, \tilde{\boldsymbol{w}}_h) \in \boldsymbol{H}_{N,h}$, solution of the analog problems (17) and (18), respectively. However, since this technique introduces unknowns where the data is known, we avoid using it to approximate the Problem (19) . Instead, we focus solely on determining the unknown quantities, which is achieved through a boundary condition homogenization technique. To this end, we define $\boldsymbol{m}_h$ as the piecewise linear continuous function such that $\boldsymbol{m}_h(\boldsymbol{x}) = \boldsymbol{0}$ for each node $\boldsymbol{x} \in \Omega \cup \Gamma_N$ and $\boldsymbol{m}_h = \boldsymbol{u}_{D,h}$ on Γ_D. Clearly, $\boldsymbol{m}_h \in [H^1_{\Gamma_N}(\Omega)]^d$. Now, invoking the *Raviart-Thomas local lifting operator on the normal trace* (cf. Proposition 2.4 in [27]), we can build $\tilde{\boldsymbol{\rho}}_{\boldsymbol{g}_h} \in H(\mathbf{div}; \Omega) \cap [\mathcal{RT}_\ell(\mathcal{T}_h)]^n$, such that $\tilde{\boldsymbol{\rho}}_{\boldsymbol{g}_h}\, \boldsymbol{n} = -\boldsymbol{g}_h$ on Γ_N.

Then, we consider $\hat{\boldsymbol{\rho}} := \tilde{\boldsymbol{\rho}} + \tilde{\boldsymbol{\rho}}_{\boldsymbol{g}_h}$ in Ω and $\hat{\boldsymbol{w}} := \tilde{\boldsymbol{w}} - \boldsymbol{m}_h$ in Ω. This helps us to rewrite (19) as: find $(\hat{\boldsymbol{\rho}}, \hat{\boldsymbol{w}}) \in \boldsymbol{H}_0$

$$\begin{cases} -\,\mathbf{div}(\hat{\boldsymbol{\rho}}) & = \boldsymbol{f} \,-\, \mathbf{div}(\tilde{\boldsymbol{\rho}}_{\boldsymbol{g}_h}) \quad \text{in} \quad \Omega\,, \\ \hat{\boldsymbol{\rho}} \,-\, \tilde{\boldsymbol{\rho}}_{\boldsymbol{g}_h} & = \mathbb{C}\,\varepsilon(\hat{\boldsymbol{w}} + \boldsymbol{m}_h) \quad \text{in} \quad \Omega\,, \\ \hat{\boldsymbol{w}} & = \boldsymbol{0} \quad \text{on} \quad \Gamma_D\,, \\ \hat{\boldsymbol{\rho}}\,\boldsymbol{n} & = \boldsymbol{0} \quad \text{on} \quad \Gamma_N\,, \end{cases} \tag{20}$$

Following the procedure described in Section 2, we establish the augmented variational formulation: find $(\hat{\boldsymbol{\rho}}, \hat{\boldsymbol{w}}) \in \boldsymbol{H}_0$ such that

$$A((\hat{\boldsymbol{\rho}}, \hat{\boldsymbol{w}}), (\boldsymbol{\tau}, \boldsymbol{v})) = \hat{F}(\boldsymbol{\tau}, \boldsymbol{v}), \qquad \forall\, (\boldsymbol{\tau}, \boldsymbol{v}) \in \boldsymbol{H}_0 \tag{21}$$

where bilinear form $A : \boldsymbol{H} \times \boldsymbol{H} :\to \mathbb{R}$ is the same defined in Section 2 and linear functional $\hat{F} : \boldsymbol{H} :\to \mathbb{R}$ is given by

$$\hat{F}(\boldsymbol{\tau}, \boldsymbol{v}) := F(\boldsymbol{\tau}, \boldsymbol{v}) - \kappa_1 \int_\Omega (\mathbb{C}^{-1}\tilde{\boldsymbol{\rho}}_{\boldsymbol{g}_h} + \varepsilon(\boldsymbol{m}_h)) : (\varepsilon(\boldsymbol{v}) + \mathbb{C}^{-1}\boldsymbol{\tau}) + \kappa_2 \int_\Omega \mathbf{div}(\tilde{\boldsymbol{\rho}}_{\boldsymbol{g}_h}) \cdot \mathbf{div}(\boldsymbol{\tau})$$

$$+ \int_\Omega (\mathbb{C}^{-1}\tilde{\boldsymbol{\rho}}_{\boldsymbol{g}_h} + \varepsilon(\boldsymbol{m}_h)) : \boldsymbol{\tau} - \int_\Omega \boldsymbol{\gamma}(\boldsymbol{v}) : \tilde{\boldsymbol{\rho}}_{\boldsymbol{g}_h} - \int_\Omega \boldsymbol{v} \cdot \mathbf{div}(\tilde{\boldsymbol{\rho}}_{\boldsymbol{g}_h})$$

with $F : \boldsymbol{H} :\to \mathbb{R}$ being introduced in Section 2. Under the same assumptions on the parameters κ_1 and κ_2 as before, that is $\kappa_1 \in (0, 2\mu)$ and $\kappa_2 > 0$, the problem (21) is well posed. Furthermore, the discrete scheme

$$A((\hat{\boldsymbol{\rho}}_h, \hat{\boldsymbol{w}}_h), (\boldsymbol{\tau}, \boldsymbol{v})) = \hat{F}(\boldsymbol{\tau}, \boldsymbol{v}), \qquad \forall\, (\boldsymbol{\tau}, \boldsymbol{v}) \in \boldsymbol{H}_{0,h} \tag{22}$$

is also well posed, and then a Céa's estimate can be obtained. In addition, the corresponding rate of convergence of the Galerkin scheme (22) for this particular choice of finite element subspaces, is presented in the next theorem. Previously, given $s > 0$, we introduce the notation for the broken spaces $H^s(\mathcal{T}_h) := \Pi_{T \in \mathcal{T}_h} H^s(T)$. Analogously, we introduce the vectorial and tensorial broken spaces $[H^s(\mathcal{T}_h)]^d$ and $[H^s(\mathcal{T}_h)]^{d \times d}$.

Theorem 7 *Let $(\hat{\boldsymbol{\rho}}, \hat{\boldsymbol{w}}) \in \boldsymbol{H}_0$ and $(\hat{\boldsymbol{\rho}}_h, \hat{\boldsymbol{w}}_h) \in \boldsymbol{H}_{0,h}$ be the unique solutions of problems* (21) *and* (22)*, respectively. In addition, assume that $\hat{\boldsymbol{\rho}} \in [H^t(\mathcal{T}_h)]^{d\times d}$, $\mathbf{div}(\hat{\boldsymbol{\rho}}) \in [H^t(\mathcal{T}_h)]^d$ and $\hat{\boldsymbol{w}} \in [H^{t+1}(\mathcal{T}_h)]^d$ for some $t \in (0, l+1]$, with $l \in \mathbb{Z}_0^+$. Then, there exists $\bar{C}_* > 0$, independent of h, such that there holds*

$$\|(\hat{\boldsymbol{\rho}}, \hat{\boldsymbol{w}}) - (\hat{\boldsymbol{\rho}}_h, \hat{\boldsymbol{w}}_h)\|^2_{\boldsymbol{H}} \leq \bar{C}_* \sum_{T\in\mathcal{T}_h} h_T^{2t} \left(\|\hat{\boldsymbol{\rho}}\|^2_{[H^t(T)]^{d\times d}} + \|\mathbf{div}(\hat{\boldsymbol{\rho}})\|^2_{[H^t(T)]^d} + \|\hat{\boldsymbol{w}}\|^2_{[H^{1+t}(T)]^d} \right).$$

Proof. Thanks to the ellipticity of the bilinear form A in $\boldsymbol{H}_0$, there exists a constant $C_{\mathtt{Cea}} > 0$, independent of h and λ, such that

$$||(\hat{\boldsymbol{\rho}} - \hat{\boldsymbol{\rho}}_h, \hat{\boldsymbol{w}} - \hat{\boldsymbol{w}}_h)||_{\boldsymbol{H}} \leq C_{\mathtt{Cea}} \inf_{(\boldsymbol{\tau}_h, \boldsymbol{v}_h)\in\boldsymbol{H}_{0,h}} ||(\hat{\boldsymbol{\rho}} - \boldsymbol{\tau}_h, \hat{\boldsymbol{w}} - \boldsymbol{v}_h)||_{\boldsymbol{H}}.$$

The rest relies on bounding the infimum by taking $(\boldsymbol{\tau}_h, \boldsymbol{v}_h) := (\pi_h^{\mathtt{RT}}(\hat{\boldsymbol{\rho}}), \pi_h^k(\hat{\boldsymbol{w}}))$, the standard orthogonal projection of $\hat{\boldsymbol{\rho}}$ and $\hat{\boldsymbol{w}}$ onto $H^{\boldsymbol{\sigma}}_{N,h}$ and $H^{\boldsymbol{u}}_{0,h}$, respectively. The proof follows after invoking very well known approximation properties of these projectors. We omit further details. □

Remark 8 *Since $\tilde{\boldsymbol{\rho}} = \hat{\boldsymbol{\rho}} - \tilde{\boldsymbol{\rho}}_{\boldsymbol{g}_h}$ and $\tilde{\boldsymbol{w}} = \hat{\boldsymbol{w}} + \boldsymbol{m}_h$, we introduce $\tilde{\boldsymbol{\rho}}_h := \hat{\boldsymbol{\rho}}_h - \tilde{\boldsymbol{\rho}}_{\boldsymbol{g}_h}$ and $\tilde{\boldsymbol{w}}_h = \hat{\boldsymbol{w}}_h + \boldsymbol{m}_h$ as its approximations. Then, we have*

$$||(\tilde{\boldsymbol{\rho}} - \tilde{\boldsymbol{\rho}}_h, \tilde{\boldsymbol{w}} - \tilde{\boldsymbol{w}}_h)||_{\boldsymbol{H}} = ||(\hat{\boldsymbol{\rho}} - \hat{\boldsymbol{\rho}}_h, \hat{\boldsymbol{w}} - \hat{\boldsymbol{w}}_h)||_{\boldsymbol{H}}$$

which implies that they have the same a-priori estimate of the error and a reliable a-posterior error estimator for one will be for both errors.

3.2 An a posteriori error analysis of the augmented formulation

We derive an a posteriori error estimator for (14) when it is approximated by performing a homogenization procedure.

First, we notice that given an approximation $(\tilde{\boldsymbol{\rho}}_h, \tilde{\boldsymbol{w}}_h)$ of the exact solution of Problem (19), to be defined later, it is straightforward to check that

$$||(\tilde{\boldsymbol{\sigma}} - \tilde{\boldsymbol{\rho}}_h, \tilde{\boldsymbol{u}} - \tilde{\boldsymbol{w}}_h)||_{\boldsymbol{H}} \leq ||(\tilde{\boldsymbol{\sigma}} - \tilde{\boldsymbol{\rho}}, \tilde{\boldsymbol{u}} - \tilde{\boldsymbol{w}})||_{\boldsymbol{H}} + ||(\tilde{\boldsymbol{\rho}} - \tilde{\boldsymbol{\rho}}_h, \tilde{\boldsymbol{w}} - \tilde{\boldsymbol{w}}_h)||_{\boldsymbol{H}}. \tag{23}$$

Thus, the total error is controlled by the error incurred when the boundary data is replaced by suitable polynomial approximations, plus the finite element approximation error of the problem with polynomial mixed boundary conditions, given in Theorem 7.

Remark 9 *Assuming that $\boldsymbol{g} \in [L^2(\Gamma_N)]^d$, $\boldsymbol{u}_D \in [H^1(\Gamma_D)]^d$ and proceeding similarly as in [16] (see also [10]), we can ensure that there exists $C > 0$, independent of h and λ, such that*

$$||(\tilde{\boldsymbol{\sigma}} - \tilde{\boldsymbol{\rho}}, \tilde{\boldsymbol{u}} - \tilde{\boldsymbol{w}})||_{\boldsymbol{H}} \leq C\,\mathrm{osc}, \qquad \mathrm{osc} = \left(\sum_{F\in\mathcal{F}_h^{\mathtt{N}}} \mathrm{osc}(\boldsymbol{g}, T)^2 + \sum_{F\in\mathcal{F}_h^{\mathtt{D}}} \mathrm{osc}(\boldsymbol{u}_D, T)^2 \right)^{1/2}, \tag{24}$$

where for each $F \in \mathcal{F}_h^{\mathtt{N}}$

$$\mathrm{osc}(\boldsymbol{g},T)^2 := \sum_{F\in E(T)\cap\mathcal{F}_h^{\mathtt{N}}} h_F\,||\boldsymbol{g} - \pi_h^{\ell}(\boldsymbol{g})||_{0,F}^2\,. \tag{25}$$

Concerning Dirichlet datum, in 2D case, under the assumption that $\boldsymbol{u}_D \in [H^1(\Gamma_D)]^2$*, it is possible to define* $\boldsymbol{u}_{D,h}$ *as the linear Lagrange interpolation of the function* $\boldsymbol{u}_D$*, and proceeding similarly as in [10] (see also [9]), we can ensure that there exists* $C>0$*, independent of* h *and* λ

$$\mathrm{osc}(\boldsymbol{u}_D,T)^2 := \sum_{F\in E(T)\cap\mathcal{F}_h^{\mathtt{D}}} h_F \left\| \frac{\partial \boldsymbol{u}_D}{\partial \boldsymbol{t}} - \frac{\partial \boldsymbol{u}_{D,h}}{\partial \boldsymbol{t}} \right\|_{[L^2(F)]^2}^2 . \tag{26}$$

Hereafter, we remind that given an edge e *induced by* $\mathcal{T}_h$*, and lying on* Γ*, we set* $\boldsymbol{t}$ *as the tangential vector associated to* e*. In addition,* $\frac{\partial \boldsymbol{u}_D}{\partial \boldsymbol{t}}$ *represents the tangential derivative of* $\boldsymbol{u}_D$ *along* e*. Similar meaning is given to* $\frac{\partial \boldsymbol{u}_{D,h}}{\partial \boldsymbol{t}}$*.*

For the 3D case, under the same assumption that $\boldsymbol{u}_D \in [H^1(\Gamma_D)]^3$*, we can ensure (see [10] and [9])*

$$\mathrm{osc}(\boldsymbol{u}_D,T)^2 := \sum_{F\in E(T)\cap\mathcal{F}_h^{\mathtt{D}}} h_{\mathtt{D}}\|\boldsymbol{u}_D - \boldsymbol{u}_{D,h}\|_{[H^1(F)]^3}^2\,, \tag{27}$$

where $h_{\mathtt{D}} := \max\{h_F : \ F\in\mathcal{F}_h^{\mathtt{D}}\}$*.*

Furthermore, assuming in addition that $\forall\, F\in\mathcal{F}_h^N \,:\, \boldsymbol{g}|_F \in [H^1(F)]^d$*, and* $\forall\, F\in\mathcal{F}_h^D \,:\, \boldsymbol{u}_D|_F \in [H^2(F)]^d$*, it is possible to establish that* $||(\tilde{\boldsymbol{\sigma}}-\tilde{\boldsymbol{\rho}},\boldsymbol{u}-\boldsymbol{w})||_{\boldsymbol{H}}$ *behaves at least as* $\mathcal{O}(h^{3/2})$*. This would allow us to see/treat the oscillation term as a higher order term. We point out that if datum* $\boldsymbol{g}$ *and* $\boldsymbol{u}_D$ *results to be piecewise polynomial and a continuous piecewise polynomial, respectively, there would be no oscillation terms.*

Now, taking into account the ellipticity of A on $\boldsymbol{H}_0$, we can establish that

$$C_{\mathtt{ell}}\,||(\hat{\boldsymbol{\rho}}-\hat{\boldsymbol{\rho}}_h,\hat{\boldsymbol{w}}-\hat{\boldsymbol{w}}_h)||_{\boldsymbol{H}} \;\le\; \sup_{(\boldsymbol{\tau},\boldsymbol{v})\in\boldsymbol{H}_0\setminus\{\boldsymbol{0}\}} \frac{A((\hat{\boldsymbol{\rho}}-\hat{\boldsymbol{\rho}}_h,\hat{\boldsymbol{w}}-\hat{\boldsymbol{w}}_h),(\boldsymbol{\tau},\boldsymbol{v}))}{||(\boldsymbol{\tau},\boldsymbol{v})||_{\boldsymbol{H}}}\,. \tag{28}$$

Our next aim, is to bound the supremum in (28). To this end, we require the following result.

Lemma 10 *For any* $(\boldsymbol{\tau},\boldsymbol{v})\in\boldsymbol{H}_0$*, there holds*

$$A((\hat{\boldsymbol{\rho}}-\hat{\boldsymbol{\rho}}_h,\hat{\boldsymbol{w}}-\hat{\boldsymbol{w}}_h),(\boldsymbol{\tau},\boldsymbol{v})) \;=\; R_1(\boldsymbol{\tau}) \,+\, R_2(\boldsymbol{v})\,, \tag{29}$$

where

$$\begin{aligned} R_1(\boldsymbol{\tau}) :=& -\kappa_2\int_\Omega (\boldsymbol{f}+\mathbf{div}(\hat{\boldsymbol{\rho}}_h-\tilde{\boldsymbol{\rho}}_{\boldsymbol{g}_h}))\cdot\mathbf{div}(\boldsymbol{\tau}) - \kappa_1\int_\Omega \Big(\epsilon(\hat{\boldsymbol{w}}_h+\boldsymbol{m}_h)-\mathbb{C}^{-1}(\hat{\boldsymbol{\rho}}_h-\tilde{\boldsymbol{\rho}}_{\boldsymbol{g}_h})\Big):\mathbb{C}^{-1}\boldsymbol{\tau} \\ &+\int_\Omega \Big(\epsilon(\hat{\boldsymbol{w}}_h+\boldsymbol{m}_h)-\mathbb{C}^{-1}(\hat{\boldsymbol{\rho}}_h-\tilde{\boldsymbol{\rho}}_{\boldsymbol{g}_h})\Big):\boldsymbol{\tau}\,. \end{aligned} \tag{30}$$

$$\begin{aligned} R_2(\boldsymbol{v}) :=& \int_\Omega (\boldsymbol{f}+\mathbf{div}(\hat{\boldsymbol{\rho}}_h-\tilde{\boldsymbol{\rho}}_{\boldsymbol{g}_h}))\cdot\,\boldsymbol{v} - \kappa_1\int_\Omega \Big(\epsilon(\hat{\boldsymbol{w}}_h+\boldsymbol{m}_h)-\mathbb{C}^{-1}(\hat{\boldsymbol{\rho}}_h-\tilde{\boldsymbol{\rho}}_{\boldsymbol{g}_h})\Big):\epsilon(\boldsymbol{v}) \\ &+\int_\Omega \gamma(\boldsymbol{v}):(\hat{\boldsymbol{\rho}}_h-\tilde{\boldsymbol{\rho}}_{\boldsymbol{g}_h}). \end{aligned} \tag{31}$$

Proof. First, given $(\boldsymbol{\tau}, \boldsymbol{v}) \in \boldsymbol{H}_0$, we invoke (21) to have

$$A((\hat{\boldsymbol{\rho}} - \hat{\boldsymbol{\rho}}_h, \hat{\boldsymbol{w}} - \hat{\boldsymbol{w}}_h), (\boldsymbol{\tau}, \boldsymbol{v})) \,=\, \hat{F}(\boldsymbol{\tau}, \boldsymbol{v}) \,-\, A((\hat{\boldsymbol{\rho}}_h, \hat{\boldsymbol{w}}_h), (\boldsymbol{\tau}, \boldsymbol{v}))\,.$$

The rest of the proof relies on the definition of $\hat{F}$ and A, and some algebraic manipulations. We omit further details. □

The next technical lemma allows us to visualize how we can reinterpret the term concerning the symmetry of the stress tensor, in the indicator.

Lemma 11 *For any $(\boldsymbol{\tau}, \boldsymbol{v}) \in \boldsymbol{H}$, there holds*

$$\int_\Omega \boldsymbol{\tau} : \gamma(\boldsymbol{v}) \,=\, 2\mu \int_\Omega (\mathbb{C}^{-1}\boldsymbol{\tau} - \epsilon(\boldsymbol{w})) : \gamma(\boldsymbol{v}) \qquad \forall \boldsymbol{w} \in [H^1(\Omega)]^d\,. \tag{32}$$

Proof. It is a straightforward application of the definition of the $\mathbb{C}^{-1}\boldsymbol{\tau}$ together with the orthogonality between symmetric and skew-symmetric tensor. □

As an immediate consequence of Lemmata 10 and 11, we deduce an a posteriori error estimator, which is given in the next theorem.

Theorem 12 *There exists $C_{\mathtt{rel}} > 0$, depending on α and ν, such that*

$$||(\hat{\boldsymbol{\rho}} - \hat{\boldsymbol{\rho}}_h, \hat{\boldsymbol{w}} - \hat{\boldsymbol{w}}_h)||_{\boldsymbol{H}} \,\leq\, C_{\mathtt{rel}}\, \eta\,, \tag{33}$$

with $\eta := \left(\sum_{T \in \mathcal{T}_h} \eta_T^2 \right)^{1/2}$, *where for any $T \in \mathcal{T}_h$*

$$\begin{aligned} \eta_T^2 \,:=\, & \max\{1\,, \kappa_2\}^2\, ||\hat{\boldsymbol{f}} \,+\, \mathbf{div}(\hat{\boldsymbol{\rho}}_h - \tilde{\boldsymbol{\rho}}_{\boldsymbol{g}_h})||_{0,T}^2 \\ & +\, \left\| \epsilon(\hat{\boldsymbol{w}}_h + \boldsymbol{m}_h) - \mathcal{C}^{-1}(\hat{\boldsymbol{\rho}}_h - \tilde{\boldsymbol{\rho}}_{\boldsymbol{g}_h}) \right\|_{0,T}^2 . \end{aligned} \tag{34}$$

As a result, we can easily establish the local efficiency of our estimator. To this end, we introduce, for any $T \in \mathcal{T}_h$

$$||(\boldsymbol{\tau}, \boldsymbol{v})||_{\boldsymbol{H}_T} \,:=\, \left(||\boldsymbol{\tau}||_{\mathrm{div};T}^2 \,+\, ||\boldsymbol{v}||_{1,T}^2 \right)^{1/2} \quad \forall\, (\boldsymbol{\tau}, \boldsymbol{v}) \in \boldsymbol{H}\,.$$

Theorem 13 *There exists $C_{\mathtt{eff}} > 0$, such that for any $T \in \mathcal{T}_h$*

$$\eta_T \,\leq\, C_{\mathtt{eff}}\, ||(\tilde{\boldsymbol{\rho}} - \tilde{\boldsymbol{\rho}}_h, \hat{\boldsymbol{w}} - \hat{\boldsymbol{w}}_h)||_{\boldsymbol{H}_T}\,.$$

The previous results allow us to derive the following a posteriori error estimate for problem (14).

Theorem 14 *Let $(\tilde{\boldsymbol{\sigma}}, \tilde{\boldsymbol{u}}) \in \boldsymbol{H}$ be the unique solution of problem* (14). *Define $(\tilde{\boldsymbol{\rho}}_h, \tilde{\boldsymbol{w}}_h) \in \boldsymbol{H}_h$ by*

$$\tilde{\boldsymbol{\rho}}_h := \hat{\boldsymbol{\rho}}_h - \tilde{\boldsymbol{\rho}}_{\boldsymbol{g}_h}, \qquad\qquad \tilde{\boldsymbol{w}}_h := \hat{\boldsymbol{w}}_h + \boldsymbol{m}_h,$$

where $(\hat{\boldsymbol{\rho}}_h, \hat{\boldsymbol{w}}_h) \in \boldsymbol{H}_{N,h}$ denotes the solution of the discrete problem (22), *and $(\tilde{\boldsymbol{\rho}}_{\boldsymbol{g}_h}, \boldsymbol{m}_h) \in \boldsymbol{H}_h$ are the approximations of the boundary data introduced at the beginning of Section 3.1. Under the assumptions of Theorems 12 and 13, together with Remark 3.1, there exist constants $C_{\mathtt{rel}}, C_{\mathtt{eff}} > 0$, depending on α and ν such that*

$$\|(\tilde{\boldsymbol{\sigma}} - \tilde{\boldsymbol{\rho}}_h, \tilde{\boldsymbol{u}} - \tilde{\boldsymbol{w}}_h)\|_{\boldsymbol{H}} \leq C_{\mathtt{rel}}\,(\eta + \mathrm{osc}), \qquad\qquad \frac{1}{C_{\mathtt{eff}}}\,\eta \leq \|(\tilde{\boldsymbol{\sigma}} - \tilde{\boldsymbol{\rho}}_h, \tilde{\boldsymbol{u}} - \tilde{\boldsymbol{w}}_h)\|_{\boldsymbol{H}} + \mathrm{osc}.$$

4 Numerical experiments

In this section, we present several numerical experiments illustrating the performance of the augmented mixed finite element schemes (22) to approximate (14) (see Theorem 14), and the adaptive algorithms based on the a posteriori error estimator η introduced in this work (cf. (34)).

We consider the simplest finite element subspaces, namely the conforming Raviart–Thomas space of lowest order combined with continuous piecewise linear polynomials (for short, $\mathbf{RT}_0 \times \mathbf{P}_1$), and the conforming Raviart–Thomas space of order one combined with continuous piecewise quadratic polynomials ($\mathbf{RT}_1 \times \mathbf{P}_2$), in both two and three space dimensions.

Since the oscillation term is of higher order (see Remark 9), its computation is omitted in this section. As mesh refinement strategies, we employ the *blue–green refinement procedure* in two dimensions ([34]) and the Bey refinement algorithm in three dimensions ([20]). Figure 1 illustrates the refinement of the marked elements.

The numerical experiments compare uniform and adaptive mesh refinement. In the uniform case, all mesh elements are refined, as shown in Figure 1, whereas in the adaptive case we use a refinement strategy based on Dörfler marking,[26], with parameter $\theta = 0.5$. The adaptive algorithm proposed is summarized as follows.

1. Start with a coarse mesh $\mathcal{T}_h$.
2. Solve the Galerkin scheme for the current mesh $\mathcal{T}_h$.
3. Compute η_T for each triangle $T \in \mathcal{T}_h$.
4. Consider stopping criterion and decide to finish or go to the next step.
5. Refine all element in a subset $\mathcal{M} \subset \mathcal{T}_h$ such that
$$\sum_{T' \in \mathcal{M}} \eta^2_{T'} \;\geq\; \theta^2 \sum_{T \in \mathcal{T}_h} \eta^2_T \,.$$
6. Define the resulting mesh as the new $\mathcal{T}_h$ and go to step 2.

In order to compare the results obtained on uniform and adapted meshes, and following the standard practice, we report the convergence rates in terms of the number of degrees of freedom (DOFs) rather than the mesh size h. Recall that we expect:

$$h^{\,l} \approx \mathrm{DOFs}^{-l/d}, \qquad \text{with } l = 1, 2 \text{ and } d = 2, 3.$$

We also define the efficiency index as the ratio between the total error and the estimator η. In all the examples presented in this section, we consider the parameters $\kappa_1 = \mu$ and $\kappa_2 = 1$, which constitute a feasible choice as discussed in Lemma 2. We recall that, given the Young's modulus E and the Poisson ratio ν of a linear elastic material, the corresponding Lamé parameters are defined by

$$\mu = \frac{E}{2(1+\nu)}, \qquad \lambda = \frac{E\,\nu}{(1+\nu)(1-2\nu)}.$$

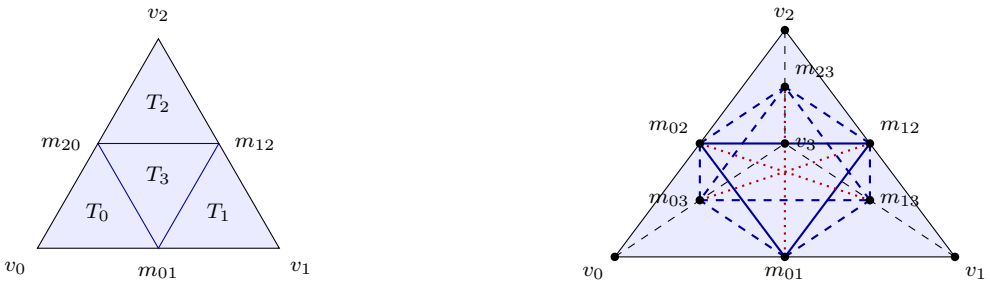

Figure 1: Refinement of marked elements in two and three dimensions using the blue–green strategy and Bey algorithm, respectively.

In the examples below, we fix $E = 1$ and consider the values $\nu = 0.4900$ and $\nu = 0.4999$, which yield the following values of μ and λ:

ν	μ	λ
0.4900	0.3356	16.4430
0.4999	0.3334	1666.4444

We now present seven numerical experiments: the first four in two dimensions and the remaining three in three dimensions. These experiments aim to confirm the theoretical results and to prove the robustness of the proposed a posteriori error estimator.

The numerical experiments were carried out using a Python implementation on a computer equipped with an Intel Ultra 7 165H processor and 32GB of DDR5 SDRAM.

4.1 Example 1. 2D Smooth solution

We first emphasize the robustness of the a posteriori error estimator η with respect to the Poisson ratio (and consequently, with respect to the Lamé constant λ). With that purpose, in the first example, we consider

$$\Omega := (0,1) \times (0,1), \qquad \Gamma_D := \{0\} \times [0,1] \qquad \Gamma_N := \partial\Omega \backslash \overline{\Gamma}_N$$

and choose the data so that the exact solution $\mathbf{u}(x_1, x_2) := (u_1(x_1, x_2), u_2(x_1, x_2))^{\mathtt{t}}$ is given by

$$u_1(x_1, x_2) = u_2(x_1, x_2) = \sin(\pi x_1)\sin(\pi x_2).$$

In Figures 2 and 3, we display the convergence of the total errors and the corresponding convergence rates (given by the slopes of the lines), together with the a posteriori error estimators and the associated efficiency indices. The results are obtained using sequences of both uniform and adaptive meshes, considering the values $\nu = 0.4900$ and $\nu = 0.4999$, together with the finite element pairs $\mathbf{RT}_0 \times \mathbf{P}_1$ and $\mathbf{RT}_1 \times \mathbf{P}_2$.

We remark that, in this case, and independently of the magnitude of the errors, there are practically no differences between the efficiency indices obtained for the two values of ν, which numerically confirms the robustness of the a posteriori error estimator η with respect to the Poisson ratio. Moreover,

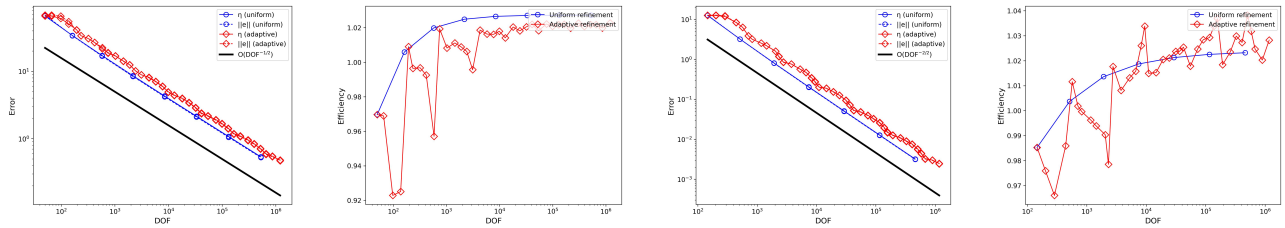

Figure 2: Example 1 (2D). Total errors and efficiency indices for uniform and adaptive refinements using $\mathbf{RT}_0 \times \mathbf{P}_1$ (left) and $\mathbf{RT}_1 \times \mathbf{P}_2$ (right), with $\nu = 0.49$.

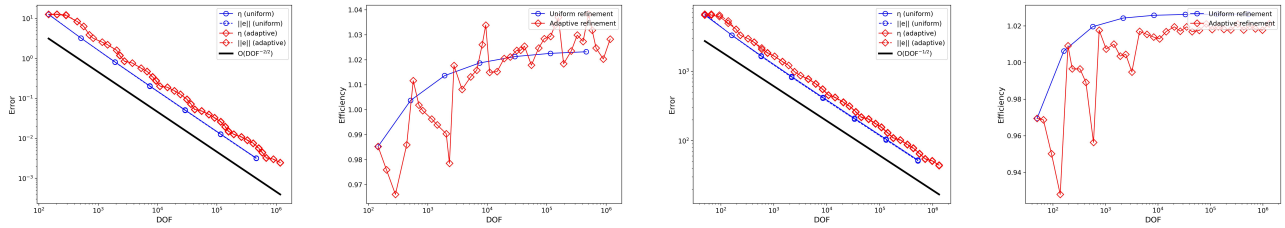

Figure 3: Example 1 (2D). Total errors and efficiency indices for uniform and adaptive refinements using $\mathbf{RT}_0 \times \mathbf{P}_1$ (left) and $\mathbf{RT}_1 \times \mathbf{P}_2$ (right), with $\nu = 0.4999$.

we observe that the efficiency indices remain bounded, staying close to 1.02, which further confirms the reliability and efficiency of η.

4.2 Example 2. 2D L-Shaped

We consider the domain $\Omega = (-1,1)^2 \, [0,1]^2$, with $\Gamma_D := (\{0\} \times [0,1]) \cup ([0,1] \times \{0\})$ and $\Gamma_N = \partial\Omega \backslash \overline{\Gamma}_D$. We take $\nu = 0.4900$, and choose the data so that the exact solution $\mathbf{u}(x_1, x_2) := (u_1(x_1, x_2), u_2(x_1, x_2))^{\mathtt{t}}$ is given by:

$$u_1(x_1, x_2) \; = \; u_2(x_1, x_2) = r^{5/3} \sin((2\theta - \pi)/3)$$

Note that the solution exhibits a singularity at the boundary point $(0, 0)$. In fact, the behaviour of $\mathbf{u}$ in a neighborhood of the origin implies that $\mathbf{div}(\boldsymbol{\sigma}) \in [H^{2/3}(\Omega)]^2$ only, which according to Theorem 7, yields $\mathcal{O}(h^{2/3})$ as the expected rate of convergence for the uniform refinement.

In Figure 4, we present the total errors, convergence rates, a posteriori error estimators, and efficiency indexes for both uniform and adaptive refinements. We observe that the errors produced by the adaptive procedure decrease much faster than those obtained with uniform refinement, as confirmed by the observed convergence rates (slopes of the corresponding lines). In the case of uniform refinement, the slope approaches $\mathcal{O}(h^{2/3})$, in agreement with the theoretical prediction. In contrast, the adaptive method is able to recover, at least approximately, the optimal rates $\mathcal{O}(\text{DOFs}^{1/2})$ for the total error with $\mathbf{RT}_0 \times \mathbf{P}_1$, and $\mathcal{O}(\text{DOFs}^{1})$ with $\mathbf{RT}_1 \times \mathbf{P}_2$. Furthermore, the efficiency indices remain

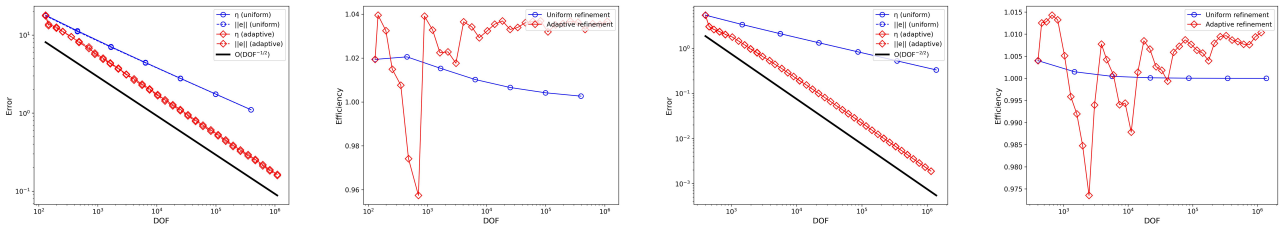

Figure 4: Example 2 (2D). Total errors and efficiency indices for uniform and adaptive refinements using $\mathbf{RT}_0 \times \mathbf{P}_1$ (left) and $\mathbf{RT}_1 \times \mathbf{P}_2$ (right), with $\nu = 0.49$.

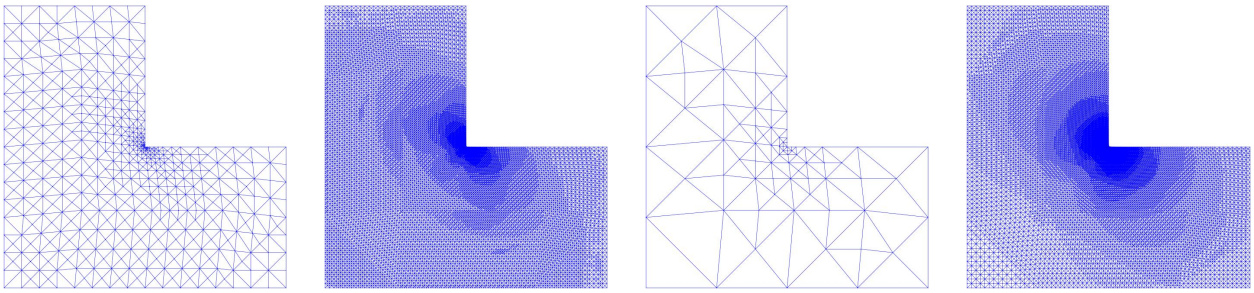

Figure 5: Example 2 (2D). Left: Adapted intermediate meshes with 4098 and 46518 DOFs for $\mathbf{RT}_0 \times \mathbf{P}_1$. Right: Adapted intermediate meshes with 1974 and 752866 DOFs for $\mathbf{RT}_1 \times \mathbf{P}_2$

bounded from above and below, which confirms the reliability and efficiency of η within the adaptive algorithm (Note the scale of the y-axis, which shows that the oscillations observed in the plot are of very small magnitude).

In addition, some intermediate meshes obtained with the adaptive refinement are displayed in Figure 5. We remark that the method is able to recognize the singularity around the singular point $(0, 0)$.

4.3 Example 3. 2D Large stress

In this example, we consider the domain $\Omega = (0, 2)^2 \backslash B[0, 1]$, with $\Gamma_D := \{\boldsymbol{x} := (x_1, x_2)^{\mathrm{t}} \in \mathbb{R}^2 : x_1^2 + x_2^2 = 1\}$ and $\Gamma_N = \partial\Omega \backslash \overline{\Gamma}_D$. The solution shows large stress regions in a neighborhood of the Dirichlet boundary Γ_D. The data are chosen so that the exact solution $\mathbf{u}(x_1, x_2)$ is given by

$$\mathbf{u}(x_1, x_2) = 5(1 - x_1^2 - x_2^2)e^{-5(1-x_1^2-x_2^2)^2}(x_1, -x_2)^{\mathrm{t}}.$$

As in the previous example, we take $\nu = 0.4900$. We note that the solution exhibits large stress concentrations in a neighborhood of the Dirichlet boundary Γ_D.

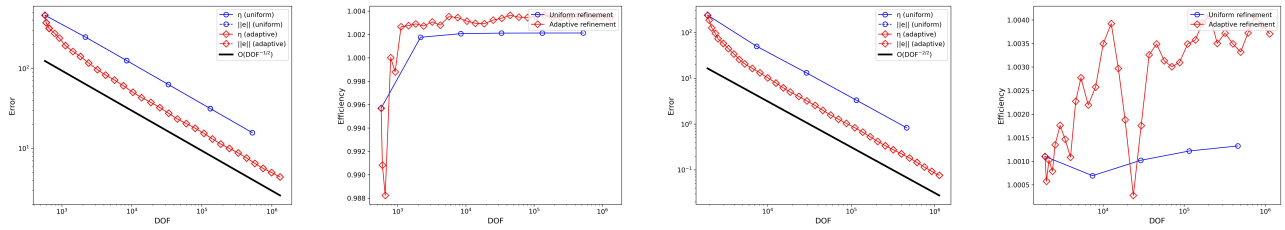

Figure 6: Example 3 (Large stress). Total errors and efficiency indices for uniform and adaptive refinements using $\mathbf{RT}_0 \times \mathbf{P}_1$ (left) and $\mathbf{RT}_1 \times \mathbf{P}_2$ (right), with $\nu = 0.49$.

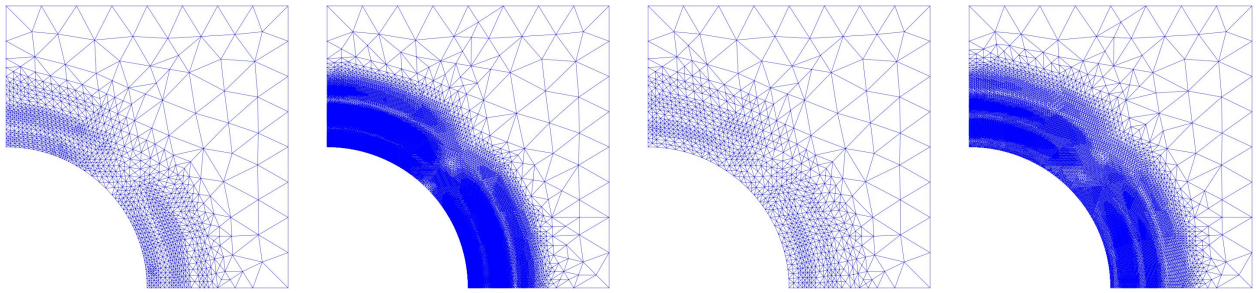

Figure 7: Example 3 (2D). Left: Adapted intermediate meshes with 13778 and 329956 DOFs for $\mathbf{RT}_0 \times \mathbf{P}_1$. Right: Adapted intermediate meshes with 29510 and 613880 DOFs for $\mathbf{RT}_1 \times \mathbf{P}_2$

In Figure 6, we display the total errors, convergence rates, a posteriori error estimators, and efficiency indices for both uniform and adaptive mesh refinements. The adaptive procedure yields a faster error reduction during the initial stages compared to uniform refinement. In both cases, the optimal convergence rates are attained: $\mathcal{O}(h) \approx \mathcal{O}(\text{DOFs}^{-1/2})$ using $\mathbf{RT}_0 \times \mathbf{P}_1$, and $\mathcal{O}(h^2) \approx \mathcal{O}(\text{DOFs}^{-1})$ when employing $\mathbf{RT}_1 \times \mathbf{P}_2$. Moreover, the efficiency indices remain uniformly bounded from above and below.

Finally, some intermediate meshes generated by the adaptive refinement procedure are displayed in Figure 7. We observe that the method successfully identifies the regions where the solution exhibits large stress concentrations.

4.4 Example 4. 2D Cooks membrane

In this example, we consider the numerical approximation of the classical Cook's membrane problem. The domain is defined by

$$\Omega := [0, 48] \times [0, 60] \setminus \left\{ (x_1, x_2) \in \mathbb{R}^2 : x_2 < \frac{11x_1}{12} \text{ or } x_2 > \frac{x_1}{3} \right\},$$

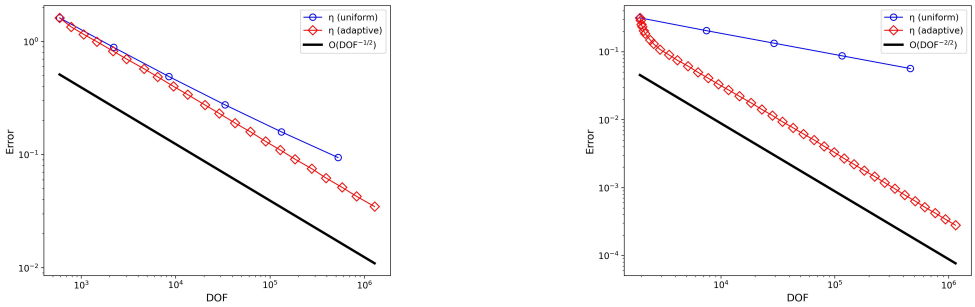

Figure 8: Example 4. 2D Cook's membrane. Total errors estimator for uniform and adaptive refinements using $\mathbf{RT}_0 \times \mathbf{P}_1$ (left) and $\mathbf{RT}_1 \times \mathbf{P}_2$ (right)

with

$$\Gamma_D := \{(x_1, x_2) \in \overline{\Omega} : x_1 = 0\}, \qquad \Gamma_N := \partial\Omega \setminus \overline{\Gamma}_D.$$

We assume homogeneous body forces, namely $\mathbf{f} = \mathbf{0}$, and prescribe the Neumann boundary condition

$$\mathbf{g}(x_1, x_2) = \begin{cases} (0,1) & \text{if } x_1 = 48 \\ (0,0) & \text{otherwise} \end{cases}$$

The material parameters are chosen as Young's modulus $E = 2900$ and Poisson's ratio $\nu = 0.3$. We analyze the convergence behavior under both uniform and adaptive mesh refinements; see Figure 8. The results show that the adaptive refinement strategy achieves a significantly faster error reduction compared to uniform refinement. Intermediate meshes obtained using the adaptive refinement strategy are shown in Figures 9 and 10. The corresponding deformations are displayed with a magnification factor of 50. We observe that the algorithm successfully identifies the regions where the solution exhibits large stress regions.

4.5 Example 5. 3D Smooth solution

We now analyze the robustness of the a posteriori error estimator η in three dimensions. We consider $\Omega := (0,1)^3$, $\Gamma_D := [0,1] \times [0,1] \times \{0\}$, $\Gamma_N := \partial\Omega \setminus \overline{\Gamma}_D$ and we choose the data so that the exact solution $\mathbf{u}(x_1, x_2, x_3)$ is given by:

$$\mathbf{u}(x_1, x_2, x_3) := (u_1, u_2, u_3)^{\mathtt{t}}, \qquad u_1 = u_2 = u_3 = x_1\, x_2\, x_3\, e^{x_1+x_2+x_3}.$$

As in Example 1, we set the Young's modulus to $E = 1$ and consider two values of the Poisson ratio, namely $\nu = 0.4900$ and $\nu = 0.4999$.

In Figures 11 and 12, we present the convergence of the total error, convergence rates, a posteriori error estimators, and efficiency indices obtained for this example using sequences of uniform and adaptive meshes for $\nu = 0.49$ and $\nu = 0.4999$, respectively. We observe that there are virtually no differences in the efficiency indices for the two values of ν, which provides strong numerical evidence

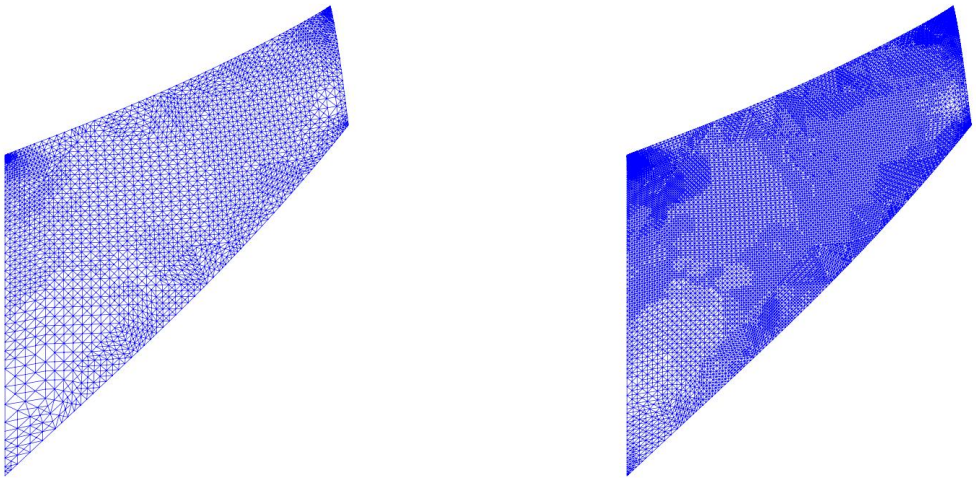

Figure 9: Example 4. 2D Cook's membrane. Adapted intermediate meshes with 29014 and 128520 DOFs using $\mathbf{RT}_0 \times \mathbf{P}_1$).

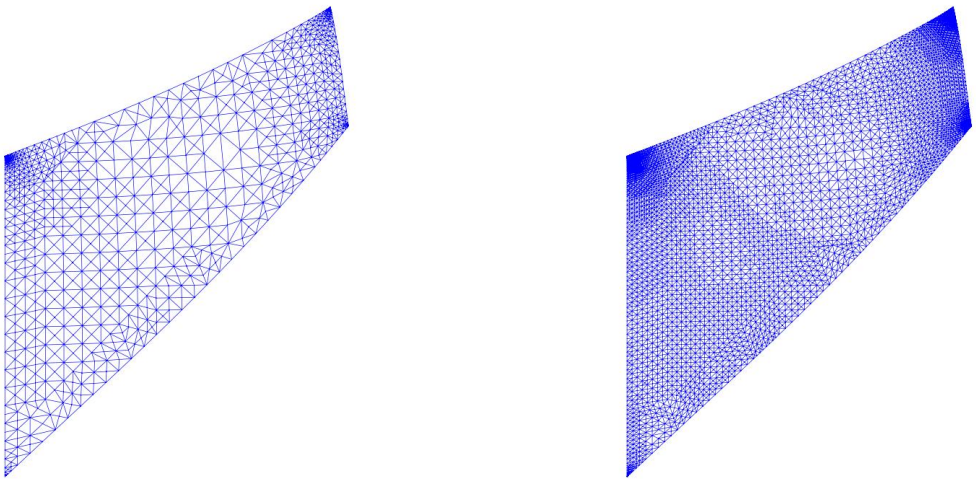

Figure 10: Example 4. 2D Cook's membrane. Adapted intermediate meshes with 28322 and 181416 DOFs using $\mathbf{RT}_1 \times \mathbf{P}_2$).

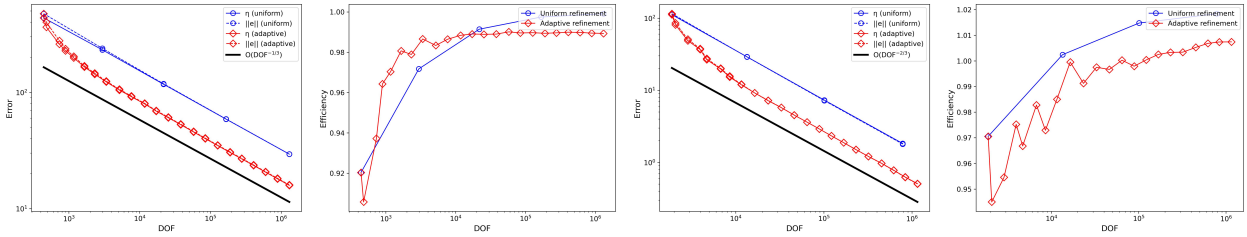

Figure 11: Example 5 (3D). Total errors and efficiency indices for uniform and adaptive refinements using $\mathbf{RT}_0 \times \mathbf{P}_1$ (left) and $\mathbf{RT}_1 \times \mathbf{P}_2$ (right), with $\nu = 0.49$.

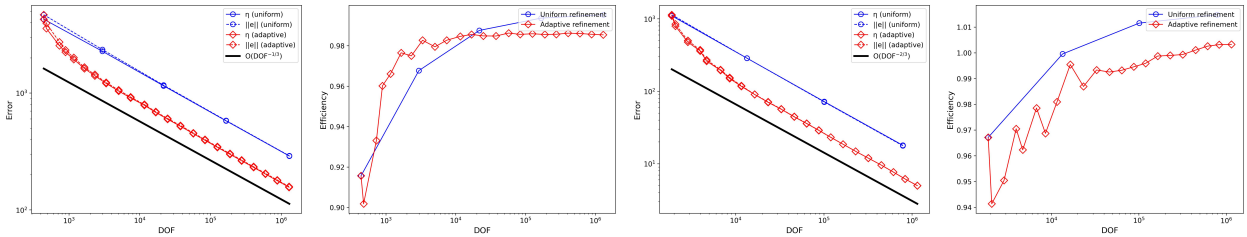

Figure 12: Example 5 (3D). Total errors and efficiency indices for uniform and adaptive refinements using $\mathbf{RT}_0 \times \mathbf{P}_1$ (left) and $\mathbf{RT}_1 \times \mathbf{P}_2$ (right), with $\nu = 0.4999$.

of the robustness of the estimator η with respect to the Poisson ratio. Moreover, the efficiency indices remain uniformly bounded and close to 1.00, in agreement with the reliability and efficiency properties of η.

4.6 Example 6. 3D Cook's membrane

In order to illustrate the performance of the adaptive algorithm based on η in a 3D domain, we extend the classical Cook's membrane by introducing a thickness of 10 units in the z-direction. We refer to the resulting 3D configuration as the Behrens' structure. In other words, the domain Ω is obtained by extruding the 2D Cook's membrane along the third spatial dimension, so that the cross-sections at $z = 0$ and $z = 10$ coincide with the original two-dimensional geometry.

We define the Dirichlet boundary as

$$\Gamma_D := \{(x_1, x_2, x_3) \in \overline{\Omega} : x_1 = 0\}, \qquad \Gamma_N := \partial\Omega \setminus \overline{\Gamma}_D.$$

We assume homogeneous body forces, $\mathbf{f} = \mathbf{0}$, and prescribe the Neumann data

$$\mathbf{g}(x_1, x_2, x_3) = \left(0, \frac{1}{16}, 0\right) \quad \text{on the portion of } \Gamma_N \text{ with } x_1 = 48,$$

while $\mathbf{g} = (0, 0, 0)$ on the remaining part of Γ_N; see Figure 13. The material parameters are chosen as Young's modulus $E = 1$ and Poisson's ratio $\nu = \frac{1}{3}$.

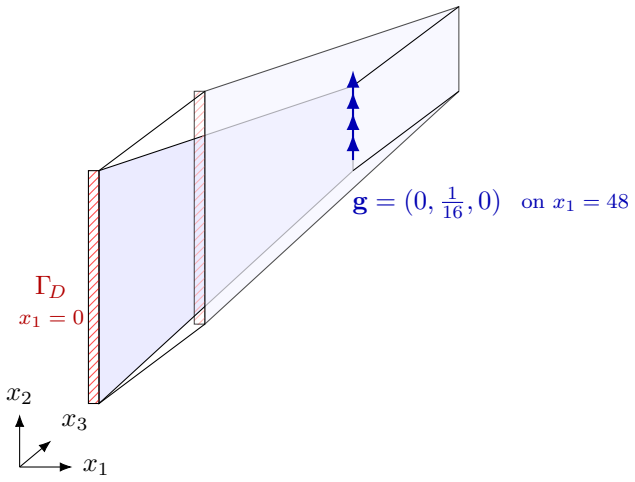

Figure 13: Example 6. Domain and boundary conditions on Behrens' structure

The total error and the error estimator η, for uniform and adaptive refinements, is displayed in Figure 17 for both pair of finite elements considered.

The total error and the error estimator η, computed using both uniform and adaptive refinements, are presented in Figure 17 for the two finite element pairs considered. Some intermediate meshes obtained via the adaptive refinement strategy are shown in Figures 18 and 19. As before, the deformations are displayed with a magnification factor of 50. We observe that the algorithm successfully identifies the regions where the solution exhibits large stress.

4.7 Example 7. 3D L-Shaped domiain

We conclude with a numerical experiment inspired by Example 1 in [1]. Let

$$\Omega := (0, 2\sqrt{2}) \times (0, 1) \times (0, 2\sqrt{2}) \setminus ((\sqrt{2}, 2\sqrt{2}) \times (0, 1) \times (\sqrt{2}, 2\sqrt{2})),$$

and define the Dirichlet boundary

$$\Gamma_D := \{(x_1, x_2, x_3) \in \partial\Omega : x_1 = 0\}, \qquad \Gamma_N := \partial\Omega \setminus \Gamma_D.$$

Homogeneous Dirichlet boundary conditions are imposed on Γ_D. We further introduce the face

$$\Gamma_F := \{\sqrt{2}\} \times (0, 1) \times (\sqrt{2}, 2\sqrt{2}).$$

We assume a vanishing body force, $\mathbf{f} = \mathbf{0}$, and prescribe the Neumann data

$$\mathbf{g} = (0, 0, 1)^{\mathrm{t}} \quad \text{on } \Gamma_F, \qquad \mathbf{g} = \mathbf{0} \quad \text{on } \Gamma_N \setminus \Gamma_F.$$

The material parameters are chosen as Young's modulus $E = 1$ and Poisson's ratio $\nu = 0.3$.

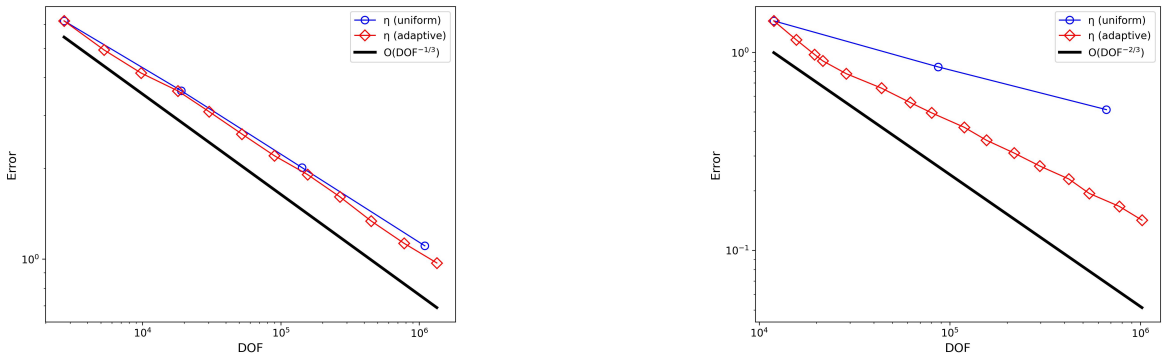

Figure 14: Example 6. 3D Cook's membrane. Total errors estimator for uniform and adaptive refinements using $\mathbf{RT}_0 \times \mathbf{P}_1$ (left) and $\mathbf{RT}_1 \times \mathbf{P}_2$ (right)

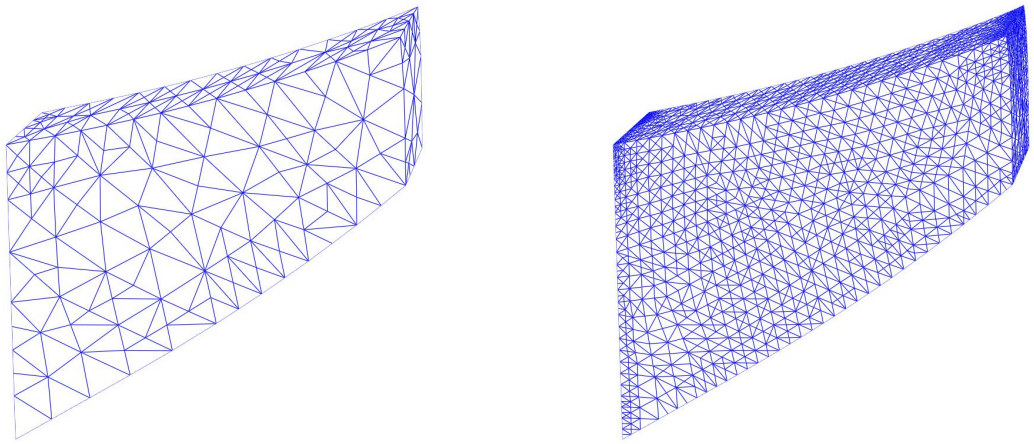

Figure 15: Example 6. 3D Cook's membrane. Adapted intermediate meshes with 18027 and 449112 DOFs using $\mathbf{RT}_0 \times \mathbf{P}_1$).

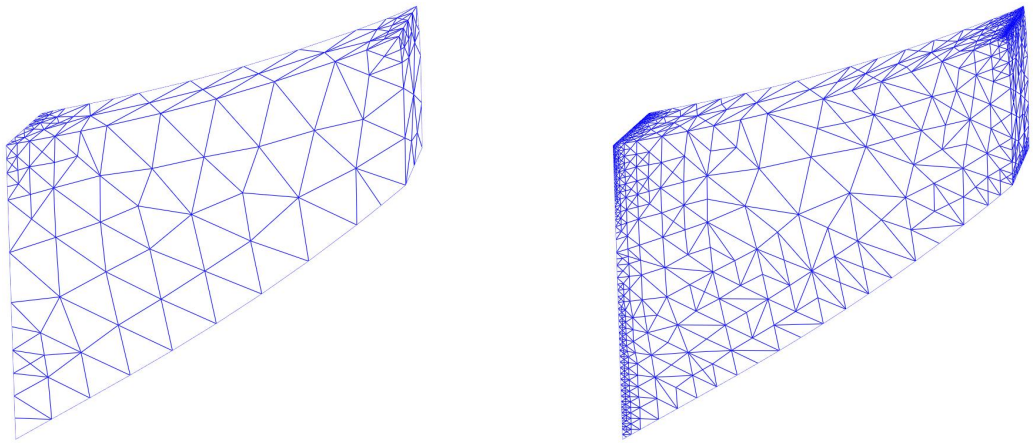

Figure 16: Example 6. 3D Cook's membrane. Adapted intermediate meshes with 43797 and 538305 DOFs using $\mathbf{RT}_1 \times \mathbf{P}_2$).

The presence of the re-entrant edge induces a singularity, which justifies the use of adaptive mesh refinement. We employ the estimator η to analyze the convergence behaviour under both uniform and adaptive refinements; see Figure 17. The results clearly indicate that the adaptive strategy achieves a significantly faster error decay than uniform refinement, while recovering the optimal convergence rate ($\mathcal{O}(DOFs^{1/3})$ for $\mathbf{RT}_0 \times \mathbf{P}_1$ and $\mathcal{O}(DOFs^{2/3})$ for $\mathbf{RT}_1 \times \mathbf{P}_2$).

Finally, some intermediates meshes obtained with the adaptive refinement are displayed in Figures 18, 19.

Summarizing, the numerical results presented in this section underline the reliability and efficiency of the error estimator η, and strongly demonstrate that the associated adaptive algorithms are much more suitable than a uniform discretization procedure when solving problems with non-smooth solutions.

Acknowledgments

The research of the first author was partially supported by Dirección de Investigación of Universidad Católica de la Santísima Concepción (Chile).

References

[1] M. Ainsworth and R. Rankin, Realistic computable error bounds for three dimensional finite element analyses in linear elasticity, *Computer Methods in Applied Mechanics and Engineering*, 200 (2011), 1909–1926.

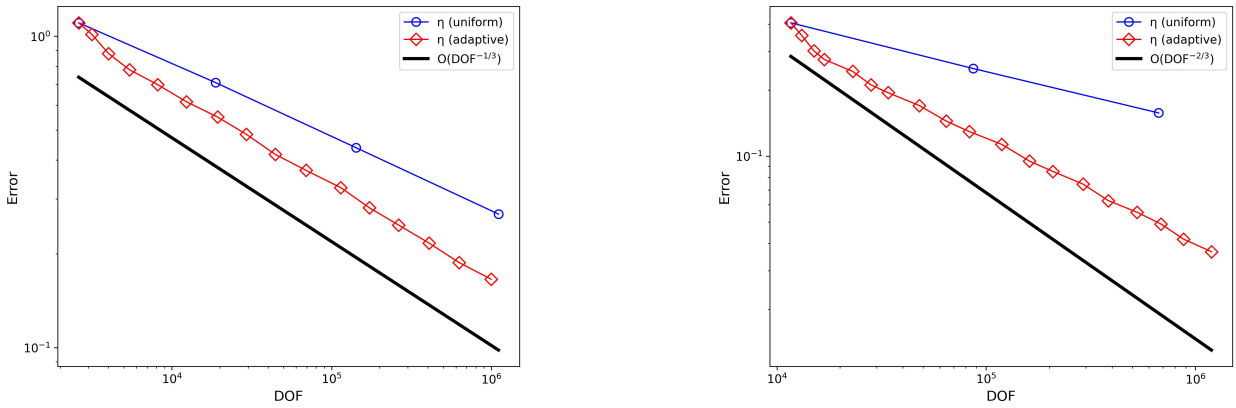

Figure 17: Example 7. 3D L-Shaped. Total errors estimator for uniform and adaptive refinements using $\mathbf{RT}_0 \times \mathbf{P}_1$ (left) and $\mathbf{RT}_1 \times \mathbf{P}_2$ (right)

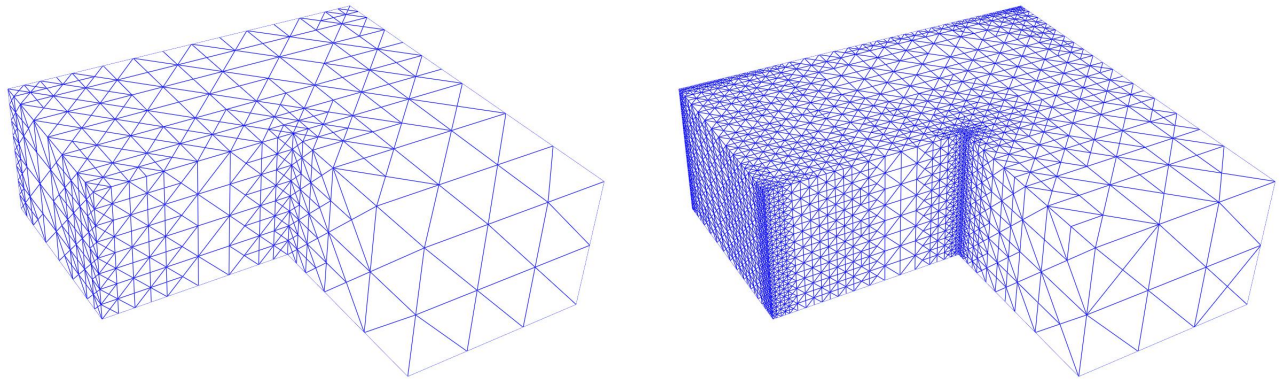

Figure 18: Example 7. 3D L-Shaped. Adapted intermediate meshes with 44385 and 627819 DOFs using $\mathbf{RT}_0 \times \mathbf{P}_1$.

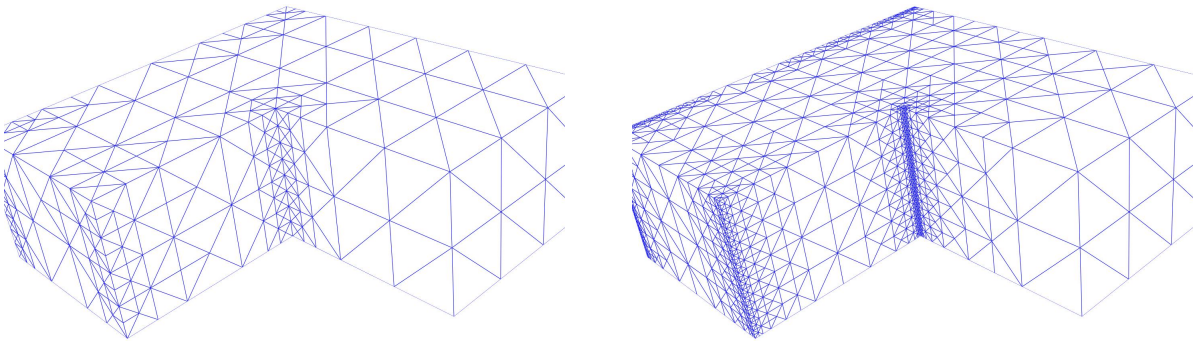

Figure 19: Example 7. 3D L-Shaped. Adapted intermediate meshes with 64377 and 526857 DOFs using $\mathbf{RT}_1 \times \mathbf{P}_2$.

[2] J. A. Almonacid, G. N. Gatica and R. Ruiz-Baier, Ultra-weak symmetry of stress for augmented mixed finite element formulations in continuum mechanics, *Calcolo*, 57 (2020), article 2.

[3] D. N. Arnold, F. Brezzi and J. Douglas Jr., PEERS: a new mixed finite element for plane elasticity, *Japan Journal of Applied Mathematics*, 1 (1984), 347–367.

[4] D. N. Arnold and R. Winther, Mixed finite elements for elasticity, *Numerische Mathematik*, 92 (2002), 401–419.

[5] D. N. Arnold, R. S. Falk and R. Winther, Differential complexes and stability of finite element methods. II: The elasticity complex, in *Compatible Spatial Discretizations*, IMA Volumes in Mathematics and its Applications, vol. 142, Springer-Verlag, 2005, 23–46.

[6] D. N. Arnold, R. S. Falk and R. Winther, Mixed finite element methods for linear elasticity with weakly imposed symmetry, *Mathematics of Computation*, 76 (2007), 1699–1723.

[7] T. P. Barrios, E. M. Behrens and R. Bustinza, An a posteriori error estimate for a dual mixed method applied to Stokes system with non null source terms, *Advances in Computational Mathematics*, 47 (2021), article 77.

[8] T. P. Barrios, E. M. Behrens and R. Bustinza, Numerical Analysis of stabilized scheme applied to incompressible elasticity problems with Dirichlet and with mixed boundary conditions, *Advances in Computational Mathematics*, 48 (2022), article 43.

[9] T. P. Barrios, E. M. Behrens and R. Bustinza, An a posteriori error estimator of the Lamé equations considering nonhomogeneous Dirichlet boundary condition, *Journal of Mathematical Analysis and Applications*, 553 (2026), article 129900.

[10] T. P. Barrios, E. M. Behrens, R. Bustinza and J. M. Cascón, An a posteriori error estimator for an augmented variational formulation of the Brinkman problem with mixed boundary conditions and non-null source terms, *Journal of Computational Physics*, 537 (2025), article 114056.

[11] T. P. Barrios, E. M. Behrens and M. González, A posteriori error analysis of an augmented mixed formulation in linear elasticity with mixed and Dirichlet boundary conditions, *Computer Methods in Applied Mechanics and Engineering*, 200 (2011), 101–113.

[12] T. P. Barrios, E. M. Behrens and M. González, Low cost a posteriori error estimators for an augmented mixed FEM in linear elasticity, *Applied Numerical Mathematics*, 84 (2014), 46–65.

[13] T. P. Barrios, E. M. Behrens and M. González, A posteriori error analysis of an augmented dual-mixed method in linear elasticity with mixed boundary conditions, *International Journal of Numerical Analysis and Modeling*, 16 (2019), 804–824.

[14] T. P. Barrios, E. M. Behrens and M. González, New a posteriori error estimator for an stabilized mixed method applied to incompressible fluid flows, *Applied Mathematics and Computation*, 351 (2019), 37–47.

[15] T. P. Barrios, J. M. Cascón and M. González, A posteriori error analysis of a stabilized mixed finite element method for Darcy flow, *Computer Methods in Applied Mechanics and Engineering*, 283 (2015), 909–922.

[16] T. P. Barrios, J. M. Cascón and M. González, A posteriori error estimation of a stabilized mixed finite element method for Darcy flow, in *Proceedings of International conference Boundary and Interior Layers — Computational & Asymptotic Methods, BAIL 2014*, Springer LNCSE 108 (2016), 13–23.

[17] T. P. Barrios, J. M. Cascón and M. González, Augmented mixed finite element method for the Oseen problem: A priori and a posteriori error analysis, *Computer Methods in Applied Mechanics and Engineering*, 313 (2017), 216–238.

[18] T. P. Barrios, J. M. Cascón and M. González, On an adaptive stabilized mixed finite element method for the Oseen problem with mixed boundary conditions, *Computer Methods in Applied Mechanics and Engineering*, 365 (2020), 113007.

[19] T. P. Barrios, G. N. Gatica, M. González and N. Heuer, A residual based a posteriori error estimator for an augmented mixed finite element method in linear elasticity, *M2AN Mathematical Modelling and Numerical Analysis*, 40 (2006), 843–869.

[20] J. Bey, Simplicial grid refinement: on Freudenthal's algorithm and the optimal number of congruence classes, *Numerische Mathematik*, 85 (2000), 1–29.

[21] D. Braess, *Finite Elements*, 3rd ed., Cambridge University Press, 2007.

[22] F. Brezzi and M. Fortin, *Mixed and Hybrid Finite Element Methods*, Springer, 1991.

[23] J. Camaño, R. Oyarzúa, R. Ruiz-Baier and G. Tierra, Error analysis of an augmented mixed method for the Navier–Stokes problem with mixed boundary conditions, *IMA Journal of Numerical Analysis*, 38 (2018), 1452–1484.

[24] C. Carstensen and G. Dolzmann, A posteriori error estimates for mixed FEM in elasticity, *Numerische Mathematik*, 81 (1998), 187–209.

[25] P. Clément, Approximation by finite element functions using local regularisation, *RAIRO Modélisation Mathématique et Analyse Numérique*, 9 (1975), 77–84.

[26] W. Dörfler, A convergent adaptive algorithm for Poisson's equation, *SIAM Journal on Numerical Analysis*, 33 (1996), 1106–1124.

[27] S. Du and F.-J. Sayas, An invitation to the Theory of the Hybridizable Discontinuous Galerkin Method. SpringerBriefs in Mathematics, Springer Nature, Switzerland AG, 2019.

[28] G. N. Gatica, Analysis of a new augmented mixed finite element method for linear elasticity allowing RT0–P1–P0 approximations, *M2AN Mathematical Modelling and Numerical Analysis*, 40 (2006), 1–28.

[29] G. N. Gatica, R. Oyarzúa and F.-J. Sayas, Analysis of fully-mixed finite element methods for the Stokes–Darcy coupled problem, *Mathematics of Computation*, 80 (2011), 1911–1948.

[30] V. Girault and F. Hecht, Numerical Methods for Grade-Two Fluid Models: Finite-Element Discretizations and Algorithms, in *Handbook of Numerical Analysis*, Vol. XVI, North Holland, 2011, 5–207.

[31] M. González, Stabilized dual-mixed method for the problem of linear elasticity with mixed boundary conditions, *Applied Mathematics Letters*, 30 (2014), 1–5.

[32] L. R. Scott and S. Zhang, Finite element interpolation of nonsmooth functions satisfying boundary conditions, *Mathematics of Computation*, 54 (1990), 483–493.

[33] R. Stenberg, A family of mixed finite elements for the elasticity problem, *Numerische Mathematik*, 53 (1988), 513–538.

[34] R. Verfürth, A Review of A Posteriori Error Estimation and Adaptive Mesh-Refinement Techniques. Wiley-Teubner (Chichester), 1996.

[35] R. Verfürth, A review of a posteriori error estimation techniques for elasticity problems, *Computer Methods in Applied Mechanics and Engineering*, 176 (1999), 419–440.

Centro de Investigación en Ingeniería Matemática (CI^{2}MA)

PRE-PUBLICACIONES 2026

2026-06 Juan José Maulén, Fernando Roldán, Cristian Vega: *Relaxed and inertial nonlinear Forward-Backward algorithm*

2026-07 Luis Briceño-Arias, Fernando Roldán: *Optimal leveraging of smoothness and strong convexity for Peaceman-Rachford splitting*

2026-08 Fahim Aslam, Jianghao Hao, Iqra Kanwal, Mauricio Sepúlveda: *Stability and finite-time blow-up for a fractionally damped nonlinear plate equation: numerical and analytical insights*

2026-09 Fahim Aslam, Zayd Hajjej, Jianghao Hao, Iqra Kanwal, Mauricio Sepúlveda, Rodrigo Véjar: *Stability and blow-up for a suspension bridge plate model with fractional damping and memory*

2026-10 Aníbal Coronel, Fernando Huancas, Mauricio Sepúlveda: *Identification of a power-like reaction term in a reaction-diffusion SIS model*

2026-11 Esteban Henriquez, Manuel Solano: *An unfitted HDG method for a distributed optimal convection-diffusion control problem*

2026-12 Sergio Caucao, Gabriel N. Gatica, Luis F. Gatica, Cristian Inzunza: *A priori and a posteriori error analysis of a mixed FEM for stationary convective Brinkman-Forchheimer flows with variable porosity*

2026-13 Jessika Camaño, Ricardo Oyarzúa, Katherine Rojo, Segundo Villa-Fuentes: *A mixed finite element method based on pseudostress and stream-function for the Navier–Stokes problem in 2D*

2026-14 Raimund Bürger, Cipriano Escalante, Enrique D. Fernández Nieto, Jorge Moya: *A two-dimensional multilayer shallow water model of tsunami-forest interaction*

2026-15 Alonso J. Bustos, Sergio Caucao: *A posteriori error analysis of two mixed formulations for a coupled Brinkman–Forchheimer and convection-diffusion-reaction system*

2026-16 Gabriel N. Gatica, Salim Meddahi, Kevin W. Pucha-Atan, Ricardo Ruiz-Baier: *A Banach spaces-based fully mixed finite element method for the thermo-electro-hydrodynamic Boussinesq problem*

2026-17 Tomás Barrios, Edwin Behrens, Rommel Bustinza, Jose M. Cascon: *A stabilized displacement - stress formulation for a linear elasticity problema with mixed boundary conditions*

Para obtener copias de las Pre-Publicaciones, escribir o llamar a: Director, Centro de Investigación en Ingeniería Matemática, Universidad de Concepción, Casilla 160-C, Concepción, Chile, Tel.: 41-2661324, o bien, visitar la página web del centro: http://www.ci2ma.udec.cl



Centro de Investigación en
Ingeniería Matemática (CI²MA)
Universidad de Concepción

Casilla 160-C, Concepción, Chile
Tel.: 56-41-2661324/2661554/2661316
http://www.ci2ma.udec.cl